Molecular Plant
Resource Article

CellPress
PARTNER JOURNAL

Local Changes in Chromatin Accessibility and Transcriptional Networks Underlying the Nitrate Response in *Arabidopsis* Roots

José M. Alvarez[1], Tomás C. Moyano[1], Tao Zhang[2], Diana E. Gras[3], Francisco J. Herrera[4,5], Viviana Araus[1], José A. O'Brien[1], Laura Carrillo[6], Joaquín Medina[6], Jesús Vicente-Carbajosa[6], Jiming Jiang[7,8] and Rodrigo A. Gutiérrez[1,*]

[1]Pontificia Universidad Catolica de Chile, Santiago, Chile

[2]Yangzhou University, Yangzhou, China

[3]Instituto de Agrobiotecnologia del Litoral, CONICET, Santa Fe, Argentina

[4]University of California, Berkeley, CA, USA

[5]Trancura Biosciences, Inc., San Francisco, CA 94158, USA

[6]Centro de Biotecnología y Genómica de Plantas (CBGP, UPM-INIA), Universidad Politécnica de Madrid (UPM), Instituto Nacional de Investigación y Tecnología Agraria y Alimentaria (INIA), Campus de Montegancedo, 28223-Pozuelo de Alarcón, Madrid, Spain

[7]Department of Horticulture, University of Wisconsin-Madison, Madison, WI 53706, USA

[8]Department of Plant Biology and Horticulture, Michigan State University, MI 48824, USA

***Correspondence: Rodrigo A. Gutiérrez (rgutierrez@bio.puc.cl)**

https://doi.org/10.1016/j.molp.2019.09.002

ABSTRACT

Transcriptional regulation, determined by the chromatin structure and regulatory elements interacting at promoter regions, is a key step in plant responses to environmental cues. Nitrate (NO_3^-) is a nutrient signal that regulates the expression of hundreds of genes in *Arabidopsis thaliana*. Here, we integrate mRNA sequencing, genome-wide RNA polymerase II (RNPII), chromatin immunoprecipitation sequencing, and DNase sequencing datasets to establish the relationship between RNPII occupancy and chromatin accessibility in response to NO_3^- treatments in *Arabidopsis* roots. Genomic footprinting allowed us to identify *in vivo* regulatory elements controlling gene expression in response to NO_3^- treatments. NO_3^--modulated transcription factor (TF) footprints are important for a rapid increase in RNPII occupancy and transcript accumulation over time. We mapped key TF regulatory interactions and functionally validated the role of NAP, an NAC-domain containing TF, as a new regulatory factor in NO_3^- transport. Taken together, our study provides a comprehensive view of transcriptional networks in response to a nutrient signal in *Arabidopsis* roots.

Key words: nitrate, transcriptional regulation, footprinting, RNA polymerase II, regulatory networks

Alvarez J.M., Moyano T.C., Zhang T., Gras D.E., Herrera F.J., Araus V., O'Brien J.A., Carrillo L., Medina J., Vicente-Carbajosa J., Jiang J., and Gutiérrez R.A. (2019). Local Changes in Chromatin Accessibility and Transcriptional Networks Underlying the Nitrate Response in *Arabidopsis* Roots. Mol. Plant. **12**, 1545–1560.

INTRODUCTION

Plants are sessile organisms that cannot relocate to find their optimal living conditions. In order to cope with a changing environment, plants rapidly adjust gene expression, metabolism, and physiology to optimize their growth, development, and reproduction. Nitrogen (N) nutrient availability is a strong environmental factor that affects many plant processes. Nitrate (NO_3^-) is the main N source for many plants and acts as a signal that regulates global gene expression, metabolism, physiology, and growth and development. In *Arabidopsis thaliana*, NO_3^- induces a rapid, broad-range modulation of gene expression that affects a myriad of genes (Alvarez et al., 2012; Krapp et al., 2014; Krouk et al., 2010a; Medici and Krouk, 2014; O'Brien et al., 2016; Vidal et al., 2015).

Despite recent advances in the identification of transcription factors (TFs) that regulate nitrate-responsive genes, there is still relatively little known about TF–target *in vivo* interactions to mediate transcriptional responses to NO_3^- in plants. TF–target binding

Published by the Molecular Plant Shanghai Editorial Office in association with Cell Press, an imprint of Elsevier Inc., on behalf of CSPB and IPPE, SIBS, CAS.

data from high-throughput heterologous approaches such as yeast-one-hybrid (Y1H) (Gaudinier et al., 2018) and *in vitro* approaches such as DNA affinity purification sequencing (DAP-seq) (O'Malley et al., 2016) have contributed to construct transcriptional networks in response to NO_3^- (Gaudinier et al., 2018; Varala et al., 2018). However, TF–target interactions identified by these methods fail to account for features present *in vivo,* such as protein–protein interactions, TF combinations, and chromatin structure. To date, only a handful of TFs, including TGA1, bZIP1, TCP20, HRS1, and NLP6/7, have been identified and found to directly bind *in vivo* to the promoter regions of cognate nitrate-responsive target genes (Konishi and Yanagisawa, 2013; Marchive et al., 2013; Alvarez et al., 2014; Guan et al., 2014; Para et al., 2014; Maeda et al., 2018). Although some of these transcription factors have been proposed as master regulatory factors, the relative importance, contribution, or position of each known TF in the nitrate transcriptional regulatory network has not been objectively assessed at a genome-wide scale.

The DNase I hypersensitivity-sequencing assay (DNase-seq) has greatly assisted identification of genome-wide *cis*-regulatory sequences and TF occupancy in different organisms (Boyle et al., 2008a; Hesselberth et al., 2009; Zhang et al., 2012a, 2012b; Neph et al., 2012). Changes in DNase I cleavage patterns have been observed at specific loci bound by TFs, supporting the finding that TFs disrupt chromatin accessibility. The single-base-pair resolution digestion patterns from DNase-seq can identify footprints of local DNA protection that accurately predict TF–DNA binding (Hesselberth et al., 2009; Boyle et al., 2011; Pique-Regi et al., 2011; Sullivan et al., 2014). Thus, in a single experiment, DNase-seq can identify both large open chromatin regions and fine-resolution TF binding sites within DNase I hypersensitive sites (DHSs).

We integrated RNA sequencing (RNA-seq), RNA polymerase II (RNPII) occupancy, and genome-wide identification of DHSs in order to analyze the relationship between regulatory DNA sequences, RNPII presence, and gene expression. We found that rapid changes in RNPII occupancy in response to NO_3^- correlate with changes in transcript accumulation. We found that changes in TF footprints in response to NO_3^- also correlate with changes in RNPII and mRNA levels at gene loci. We analyzed the relative contribution of known and new TFs in NO_3^- regulation of target genes by integrating genomic footprinting, transcriptional regulation of gene expression based on RNPII occupancy, and transcriptome data. These datasets provide an unbiased scaffold *in vivo* to propose a NO_3^- transcriptional regulatory network holding TFs, *cis*-regulatory elements, and cognate target genes that make up the rapid response *Arabidopsis* roots to NO_3^-.

RESULTS

Chromatin Accessibility Correlates with mRNA Levels and RNPII Occupancy in *Arabidopsis* Roots

To generate a transcriptional landscape of the *A. thaliana* root and to study the relationship between gene expression and chromatin accessibility in response to NO_3^- treatments, we evaluated gene expression by RNA-seq, RNPII occupancy by chromatin immunoprecipitation sequencing (ChIP-seq) and mapped DHSs by DNase-seq in NO_3^--treated and control roots of *A. thaliana* Col-0 plants. Plants were grown hydroponically for 2 weeks with 0.5 mM ammonium succinate as the only N source. At dawn on day 15, plants were exposed to 5 mM KNO_3 or 5 mM KCl as a control. We and other research groups have used this experimental design to elicit fast and robust responses to NO_3^- treatments in *A. thaliana* (Wang et al., 2000, 2004; Krouk et al., 2010b; Alvarez et al., 2014). Roots were harvested for RNA isolation, and polyA$^+$ enriched fractions were used to construct libraries for RNA-seq. We performed ChIP-seq for RNPII using specific antibodies (Ab817, Abcam) previously tested in ChIP experiments in *A. thaliana* (Saze et al., 2013). We analyzed chromatin accessibility patterns by developing DNase-seq libraries from root and identified DHSs using the F-seq software (Boyle et al., 2008b). As a reference, we also used naked DNA, which is a sample stripped of proteins, digested with DNase I, and sequenced.

Previous studies in *Arabidopsis* whole seedlings have shown a positive correlation between RNPII occupancy and mRNA levels (Alexandre et al., 2018; Zhang et al., 2012b). To assess the relationship between RNPII occupancy and gene expression in *Arabidopsis* roots, we plotted normalized RNPII read counts within ±1000 bp of transcription start sites (TSSs) in genes that were binned according to transcript levels using our RNA-seq data. Genes with high transcript abundance showed higher RNPII occupancy than genes with lower transcript abundance (Figure 1A). RNPII was found positioned immediately downstream of the TSS, an occupancy pattern consistent with previous studies in *A. thaliana* and humans (Chodavarapu et al., 2010; Welboren et al., 2009; Zhang et al., 2012b). Previous studies have shown a positive correlation between chromatin accessibility and RNPII occupancy (Alexandre et al., 2018). To assess the relationship between chromatin accessibility and RNPII occupancy in *Arabidopsis* roots, we plotted normalized DNase-seq read counts within ±1000 bp of TSS, where genes were binned according to levels of RNPII occupancy. Consistent with previous plant studies (Alexandre et al., 2018; Rodgers-Melnick et al., 2016; Zhang et al., 2012b), chromatin accessibility was found to peak immediately upstream of the TSS (Figure 1B). Genes with higher RNPII occupancy showed higher DNase-seq reads than genes with lower RNPII occupancy (Figure 1B). A representative gene is shown in Figure 1C. *At4g05390* codes for a root-type ferredoxin:NADP(H) oxidoreductase (RFNR1) that is highly expressed in roots. We found high levels of RNPII bound throughout the *RFNR1* gene body (Welboren et al., 2009; Chodavarapu et al., 2010) (Figure 1C), consistent with *RFNR1* active transcription in roots under our experimental conditions. We also found high levels of chromatin accessibility in the promoter of *RFNR1* (Figure 1C).

These results show genome-wide correlation between accessible chromatin regions and mRNA levels in root organs and suggest a functional association between open chromatin and RNPII occupancy indicative of transcriptional control.

Nitrate Triggers Rapid Changes in RNPII Occupancy in Nitrate-Responsive Genes

Changes in gene expression in response to NO_3^- and other signals have been mainly evaluated by measuring transcript

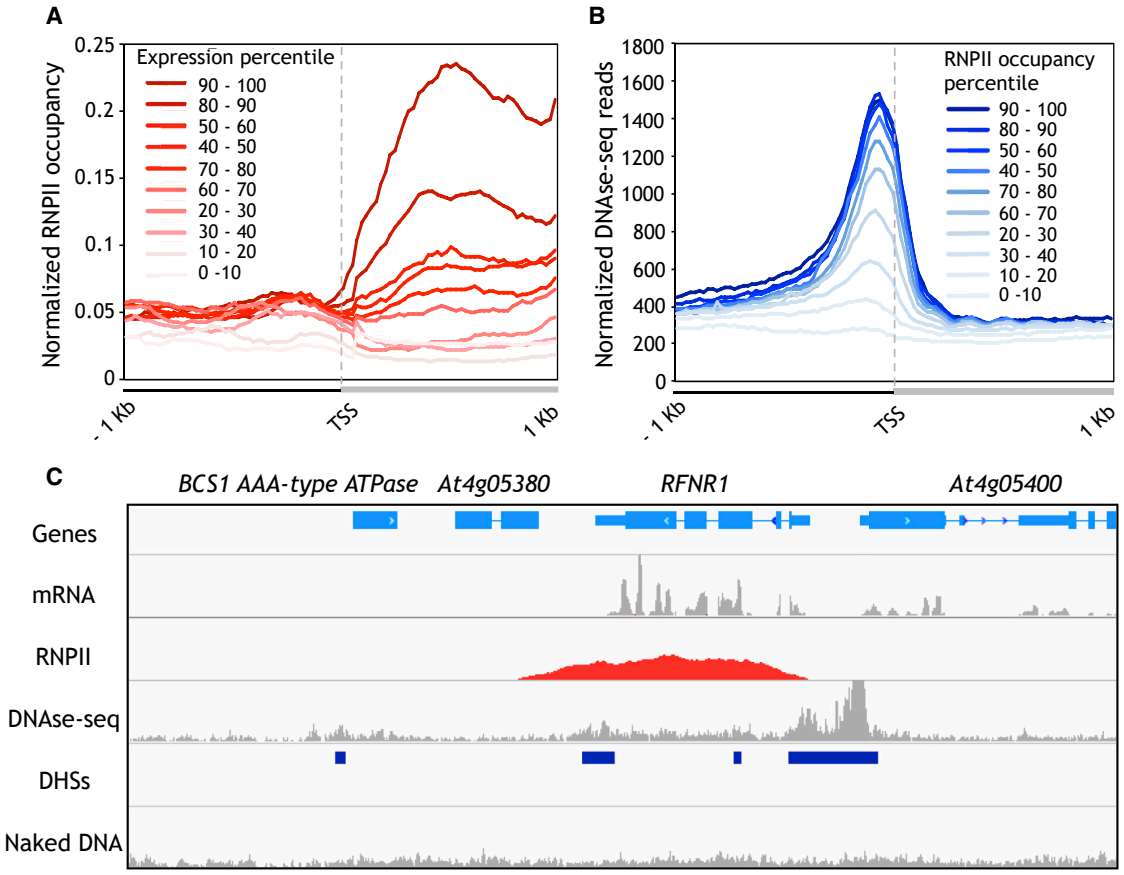

Figure 1. Highly Expressed Genes Show High Levels of RNPII and Chromatin Accessibility in Roots.

(A) Percentage of genes with different expression levels associated with RNPII occupancy in the 1000-bp upstream regions of the TSS to the 1000-bp downstream regions of the TSS. Genes were divided into 10 bins based on their expression levels from 0% to 100%.

(B) Profile of DNase I sensitivity, indicated by the number of normalized DNase-seq reads among the genes with different RNPII occupancy levels. Genes were divided into 10 bins from low RNPII occupancy (0%) to high RNPII occupancy (100%), based on the occupancy levels.

(C) Representative example of a highly expressed gene showing high RNPII occupancy and high DNase-seq reads in the promoter. Shown is the genomic context of *FNR1* gene with tracks denoting gene models, RNA-seq reads, ChIP-seq reads for RNPII, DNase-seq reads, DHSs detected in DNase-seq library from roots, and naked DNA control reads.

abundance, using microarrays or RNA-seq technologies (reviewed in Krouk et al., 2010a; Tsay et al., 2011; Vidal and Gutierrez, 2008). However, RNPII occupancy throughout the gene provides a direct readout of potential transcriptional activity, which is not possible by profiling mRNA expression. To assess the genome-wide RNPII occupancy in response to NO_3^- treatments, we performed ChIP-seq experiments in plants treated with 5 mM KNO_3 or KCl for 12 min. We chose this time point because previous studies have reported that 12 min is the earliest time point in which regulation of gene expression for a sizable subset of nitrate-responsive genes can be detected (Krouk et al., 2010b). We determined the $\log_2$ ratio of KNO_3/KCl to identify genome-wide changes in RNPII occupancy in response to NO_3^-. At a genome-wide scale, RNPII occupancy changed significantly for 337 genes in response to NO_3^- treatments (1.5-fold change in occupancy level, $p < 0.05$), with 317 genes showing an increase and 20 genes showing a decrease in RNPII occupancy (Figure 2A) (Supplemental Table 1). Genes showing an increase in RNPII occupancy overlapped significantly with transcripts induced by NO_3^- at 12, 20, 60, and 120 min after NO_3^- treatments according to our mRNA-seq experiment (overlap ranging from 33% to 69%, $p < 0.001$) (Supplemental Figure 1A; the complete list of transcripts regulated at different time points is provided in Supplemental Table 2). A high and significant proportion of genes showing an increase in RNPII occupancy or mRNA levels are regulated directly by nitrate and not by downstream metabolites (Supplemental Figure 1B). We found a low overlap for genes showing a decrease in RNPII occupancy by NO_3^- and transcript repression (overlap ranging from 1.5% to 4%) (Supplemental Figure 1A). We found that NO_3^- triggered a significant increase in RNPII occupancy in 31 of 45 genes (69% of genes) regulated at the transcript level at the same time point (Figure 2B). We did not find a full overlap between genes showing an increase in both RNPII and transcript levels at 12 min. We may have missed moderate but relevant changes in RNPII occupancy for the control gene expression because we favored a stringent statistical analysis (Supplemental Figure 2). In addition, post-transcriptional control mechanisms may also play a role in the control of transcript abundance in response to nitrate as described previously (Gifford et al., 2008; Vidal et al., 2010, 2013a).

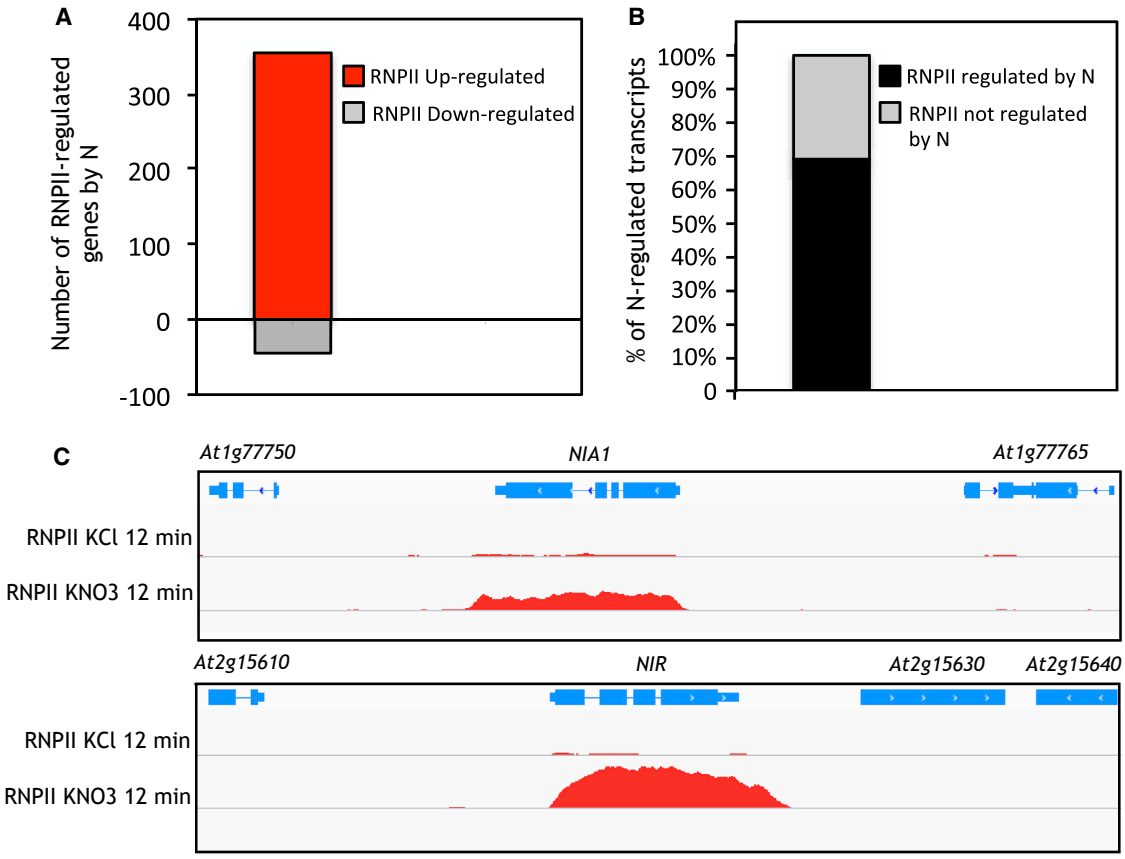

Figure 2. NO_3^- Triggers Rapid Changes in RNPII Patterns.
(A) 317 genes show a significant increase in RNPII occupancy in response to NO_3^- treatments and 20 genes show a decrease in RNPII occupancy. More genes are upregulated than downregulated at RNPII occupancy level ($p < 1E{-}13$, 2-sample test for equality of proportions with continuity correction).
(B) 69% of transcripts induced by NO_3^- show a significant increase in RNPII occupancy in response to NO_3^-. 69% is a significant proportion compared with genes with RNPII not regulated by N ($p < 0.0008$, 2-sample test for equality of proportions with continuity correction).
(C) RNPII occupancy increases in *NIA1* and *NIR* genes in response to NO_3^-.

Of the 317 genes with increased RNPII at 12 min, 279 (88%) showed mRNA accumulation at 12 min or later time points (Supplemental Figure 1C). Induced changes in RNPII occupancy with no changes in transcript may reflect transcriptionally activated genes for which mRNA is synthesized but rapidly degraded (Marguerat et al., 2014; Mokry et al., 2012). Consistently, we found that transcript accumulation of a proportion of NO_3^--responsive genes is highly transient (Supplemental Figure 3), as previously described (Krouk et al., 2010b). Despite some discrepancies, we found that the magnitude of RNPII occupancy highly correlated (0.71) with levels of transcript accumulation in response to NO_3^- treatments (Supplemental Figure 4).

Figure 2C shows the genomic context of the prototypical nitrate-responsive gene *NITRATE REDUCTASE 1* (*NIA1*), a gene whose product is involved in the first step of NO_3^- reduction (Cheng et al., 1988). We found *NIA1* shows a clear increase in RNPII occupancy in response to NO_3^- treatments compared with KCl treatments. The *NITRITE REDUCTASE* (*NIR*) also showed an increase in RNPII occupancy at 12 min of exposure to NO_3^- (Figure 2C).

These results indicate that NO_3^- treatments trigger rapid genome-wide changes in RNPII occupancy, which correlate with early, transient, and late changes at the mRNA level in roots under our experimental conditions.

Chromatin Accessibility Patterns Are Stable during Rapid Nitrate Responses

We found between 30 030 and 36 395 DHSs per sample using a stringent false discovery rate (FDR) threshold (<0.05). We calculated the Signal Portion of Tags (SPOT) score, which measures signal-to-noise as the fraction of cuts within DHS in each DNase-seq library (Alexandre et al., 2018). This analysis reveals the quality of our DNase-seq data (Supplemental Table 3). Chromatin accessibility profiles are reported to be highly reproducible (Sabo et al., 2006; Sullivan et al., 2014; Alexandre et al., 2018). Indeed, we found a high correlation between biological replicates (Supplemental Figure 5, Supplemental Table 3) and approximately 92%–95% of the identified DHSs were reproducible between biological replicates (Supplemental Table 3). These results confirm the high reliability of the DNase-seq method and the high quality of our datasets.

We found NO_3^- induces rapid changes in RNPII occupancy (Figure 2) and highly transcribed genes exhibit high levels of

chromatin accessibility (Figure 1B). However, it is unclear whether NO_3^- induces changes in chromatin accessibility affect transcription during rapid responses. To address this question, we determined the chromatin state after NO_3^- treatments and compared it with the chromatin state before the treatment (time 0) and after KCl control treatments. We first compared DNase I cut counts within DHSs to identify differential DHSs after NO_3^- treatments genome-wide using DESeq2 (Love et al., 2014). We found marginal effects of the 12-min NO_3^- treatment compared with time 0 or after KCl control treatment (Supplemental Figure 6A and 6B). For example, only one differential DHS (log2 fold change >1.5) was found by comparing NO_3^- treatment with KCl treatment (Supplemental Figure 6A; Supplemental Table 4). Similar results were found by comparing NO_3^- treatment with the time 0 control (Supplemental Figure 6B, Supplemental Table 4). We also tested whether nitrate-responsive DHSs identified by DESeq2 change by subsampling the libraries to the same number of reads to the library with lower read depth. We found the results do not change by subsampling the libraries (Supplemental Figure 6C and 6D, Supplemental Table 4). These results indicate NO_3^- treatments do not change the overall chromatin accessibility patterns.

In addition, we determined the chromatin state after NO_3^- treatments and compared it with control treatments for those genes that exhibited changes in RNPII occupancy in response to NO_3^-. Specifically, we analyzed DNase I sensitivity levels in the 1000-bp regions upstream from the TSS because (1) they contain a high percentage of DHSs according to our data (Supplemental Figure 7) and (2) previous DNase-seq studies have shown that they contain most of the *cis*-regulatory elements in *A. thaliana* (Sullivan et al., 2014; Zhang et al., 2012b). We sorted genes based on fold changes of RNPII occupancy (KNO_3/KCl) and found similar chromatin accessibility patterns at time 0 compared with 12 min of NO_3^- or KCl treatments in the 1000-bp regions upstream from the TSS (Figure 3A). These results indicate that increased or decreased RNPII occupancy occurs without obvious changes in DNase I sensitivity patterns at promoter regions after NO_3^- treatments (Figure 3A). We found that NO_3^- treatments do not change the number of DHSs or the DNase-seq reads compared with time 0 or KCl control (Figure 3B and 3C). To investigate whether longer treatments could influence DNase I sensitivity, we performed similar analysis using 2 h of NO_3^- or KCl treatment as a control, a timeframe in which the nitrate response is well established with over 1000 regulated genes (Krouk et al., 2010b; Alvarez et al., 2014). We found chromatin accessibility does not change either after 2 h of NO_3^- treatments (Supplemental Figure 8A) on NO_3^--regulated genes under our experimental conditions or genome-wide (Supplemental Figure 8B).

These results indicate NO_3^- does not change overall chromatin accessibility patterns in the promoter of transcriptionally regulated genes, and only a marginal effect genome-wide was observed during rapid responses to this environmental signal. RNPII activity and specific TFs are important contributors for rapid changes in root gene expression in response to nitrate treatments, as described below.

Footprinting Patterns within DHSs Are Indicative of Transcriptional Control in Response to Nitrate Treatments

Local changes in chromatin accessibility caused by TF binding have been described previously in response to environmental stimuli (John et al., 2011; Sullivan et al., 2014; Liu et al., 2017b). We investigated whether NO_3^- treatments in roots produce local changes in TF footprinting within DHSs using our DNase-seq data. We considered a NO_3^--modulated footprint as one in which a given *cis*-acting element was differentially detected in KNO_3- versus KCl-treated samples. Using this criterion, we found 6001 NO_3^--modulated footprints mapped within the promoters of 2740 genes (Supplemental Table 5). Genes that show increased RNPII occupancy in response to NO_3^- treatments overlapped significantly with genes with NO_3^--modulated footprints (Figure 4A). Moreover, a significant proportion of genes whose transcript levels are induced by NO_3^- overlapped with genes with NO_3^--modulated footprints (Figure 4A). Thus, NO_3^--modulated footprints promoted by NO_3^- correlated well with increased RNPII occupancy and transcript levels over time. However, we found no significant overlap for nitrate-modulated footprints with genes that are repressed by NO_3^- as determined by RNPII occupancy and mRNA levels (Figure 4A). These results suggest changes in footprinting patterns may not be directly related to rapid transcriptional repression under our experimental conditions.

Nitrate-modulated footprints can be associated with protein recruitment or disengagement in response to nitrate treatments depending on whether the footprint was found in KNO_3- or KCl-treated samples. We mapped both types of footprints within the 1000-bp regions upstream of TSS for genes that show increased RNPII occupancy in response to NO_3^- treatments. The resulting distribution indicates that a high proportion of the footprints are located between 300 bp and the TSS (Figure 3B and 3C). A representative example of a nitrate-modulated footprint is shown in the promoter of *ACR12*, a gene involved in amino acid synthesis (Sung et al., 2011) (Supplemental Figure 9). This footprint corresponds to the *cis*-acting motif of TGA1, a known bZIP TF involved in gene expression in response to NO_3^- (Supplemental Figure 9). TFs belonging to different gene families are recruited or disengaged by NO_3^- treatments, with important contributions from bZIP and BBR-BPC transcription factor families, respectively (Supplemental Figure 10).

These findings indicate that the differential TF binding of DNA sequences close to the TSS, due to TF recruitment or TF disengagement in response to NO_3^-, is an important component in transcriptional control of gene expression in response to NO_3^-. Notwithstanding, we also found footprints from TFs that are bound regardless of the experimental conditions (Supplemental Table 5). Among this class, we found footprints for known TFs involved in the NO_3^- response (e.g., TCP20, Supplemental Table 6).

Integrative Network Analysis Recovered Known and Identified New TFs Implicated in the Transcriptional Responses to Nitrate

To gain insight into the transcriptional regulation by NO_3^-, we integrated the data generated in a single transcriptional model. We generated a matrix with TF–target interactions where targets are

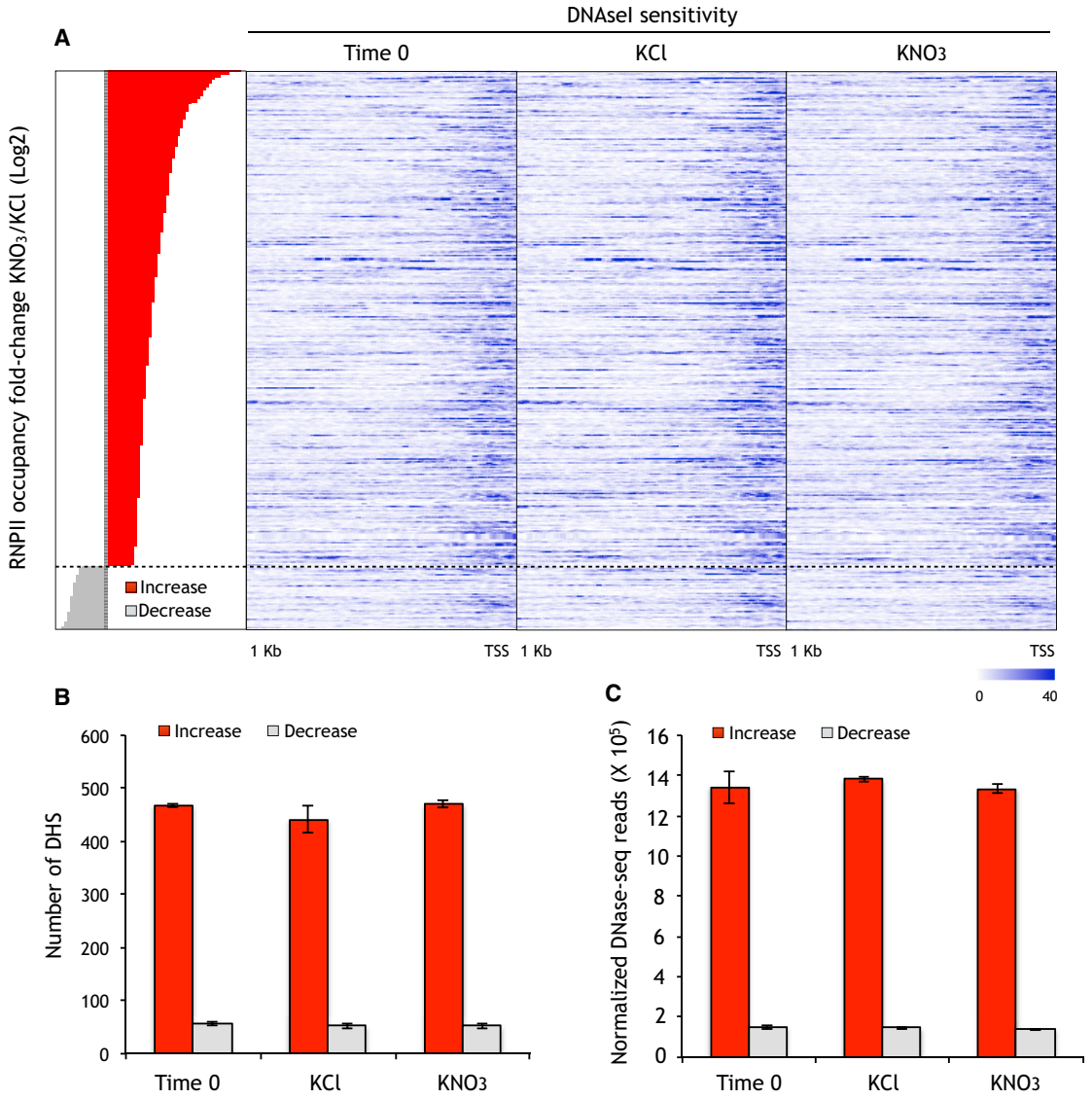

Figure 3. Chromatin Accessibility Does Not Change in Response to NO_3^- Treatments in the Promoter of Transcriptionally Regulated Genes by NO_3^-.

(A) Heatmap of DNase I sensitivity surrounding the TSSs of genes in which RNPII occupancy changes in response to NO_3^-. Genes were sorted based on fold change of RNPII occupancy of KNO_3 relative to KCl (genes in the four panels are in the same order). The RNPII occupancy of genes above/under the black-segmented line were significantly increased or decreased by NO_3^-, respectively.

(B and C) (B) Number of DHS and **(C)** DNase I sensitivity (DNase-seq read number per bp genome per million reads) in 1000-bp upstream regions of the TSS of genes showing changes in RNPII occupancy by NO_3^-.

genes for which RNPII occupancy increased with a concomitant increase of transcript levels in response to NO_3^- treatments (Supplemental Table 6). The TF–target interaction was generated when a footprint of a source TF was detected in the promoter of the target gene (Supplemental Table 6). This analysis connected 333 TFs and 134 targets (Supplemental Table 6).

Our analysis captured important TFs previously characterized as key regulatory factors in the NO_3^- response, including NLP7, TGA1, TGA4, HRS1, bZIP1, TCP20, NAC4, CCA1, and SPL9 (Alvarez et al., 2014; Castaings et al., 2009; Guan et al., 2014; Gutierrez et al., 2008; Konishi and Yanagisawa, 2013; Krouk et al., 2010b; Liu et al., 2017a; Marchive et al., 2013; Medici et al., 2015; Para et al., 2014; Vidal et al., 2013b) (Supplemental Table 6). Our *in vivo* results can also help define which TF–target interactions detected from *in vitro* TF–DNA binding experiments are functional. Specifically, our comparisons shows that a high proportion of TF–target interactions for TGA1 (4 of 5), NLP7 (2 of 5), and TCP20 (7 of 8) detected by our footprinting approach were also captured by DAP-seq (O'Malley et al., 2016) (Supplemental Table 6). On average for TFs in the DAP-seq dataset, we found 45% validation of TF–target relationships in our analysis (Supplemental Table 6). A recent approach using enhanced yeast one-hybrid assays captured 345 TFs that bind to the promoter of genes involved in N metabolism (Gaudinier et al., 2018). We captured a high and significant

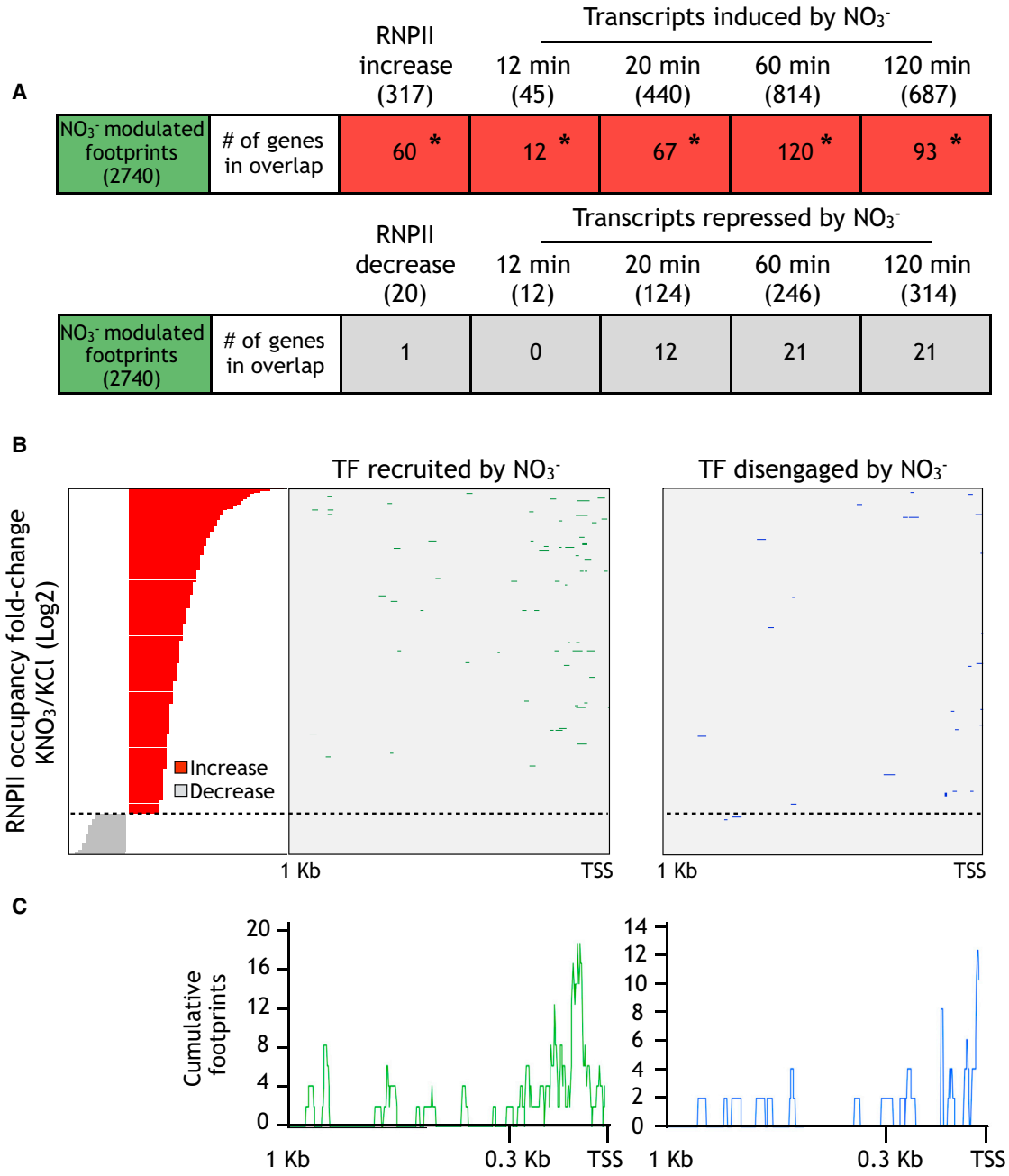

Figure 4. Nitrate Produces Rapid Changes in Transcription Factor Footprints in the Promoter of NO_3^- Induced Genes.

(A) Overlaps between genes showing NO_3^--modulated footprints and genes showing an increase or decrease in RNPII occupancy. Overlaps were also calculated for genes showing NO_3^--modulated footprints and genes induced or repressed by 12, 20, 60, and 120 min of KNO_3 treatments. The number of genes that belong to each gene list is shown in brackets below the name of the gene list. The number of genes overlapping in each comparison is indicated inside the quadrate. The *p* value of each overlap was calculated in R using Fisher's exact test. *$p < 0.001$.

(B) Distribution of footprints from TF recruited (green bars) or TF disengaged (blue bars) by NO_3^- in the 1000-bp region upstream from the TSS of genes that show increased or decreased RNPII occupancy in response to NO_3^- treatments.

(C) Accumulated distribution of footprints in the 1000-bp region upstream from the TSS of genes that show increased RNPII occupancy in response to NO_3^- treatments.

proportion of these TFs identified *in vitro* (96 of 345, $p = 3.4E{-}15$, $V = 0.21$, Fisher's exact test) (Gaudinier et al., 2018) with our integrative *in vivo* approach.

ChIP-chip assays revealed that NLP7 is bound to 851 genes after 10 min of NO_3^- treatments in roots (Marchive et al., 2013). Among the genes bound by NLP7, we captured a significant proportion (44/851, $p = 4E{-}7$, $V = 0.02$, Fisher's exact test) by our footprinting strategy. Moreover, our analysis captured previously validated regulatory interactions determined by ChIP–qPCR assays, including TCP20-*NIA1*, TCP20-*NRT1.1* (Guan et al., 2014), TGA1-*NRT2.1,* TGA1-*NRT2.2* (Alvarez et al.,

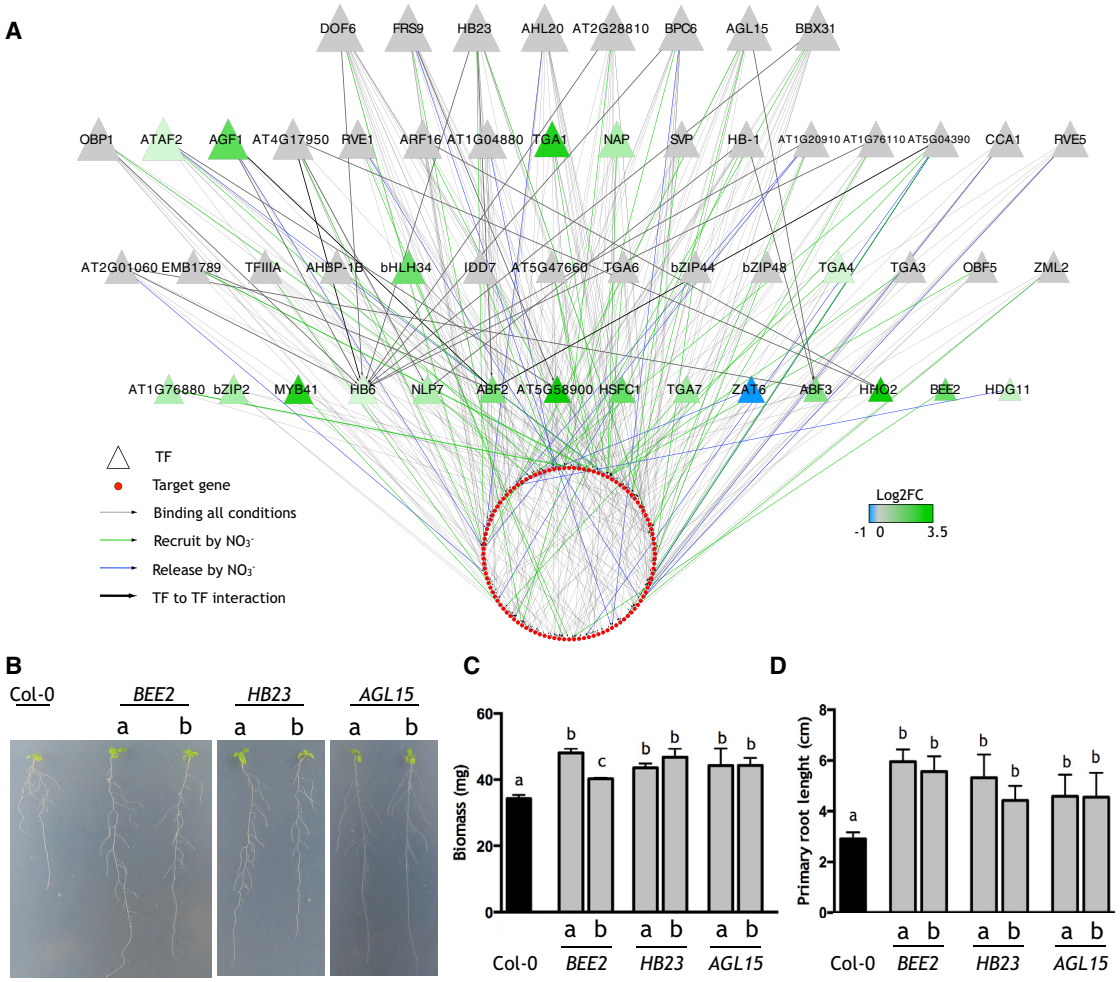

Figure 5. Transcription Factor Network Integrate Transcriptional Regulation and Connectivity Features of Genes in the NO_3^- Response.

To build the network, an edge was created when a footprint of a source TF (triangles) was detected in the promoter of the target gene (circles). Red nodes represent genes for which RNPII occupancy increased with a concomitant increase in transcript levels in response to NO_3^- treatments.

(A) Color of triangles represents TF expression levels in response to NO_3^-, according to our RNA-seq experiments. Green edges represent protein–DNA interactions from TFs that are recruited to the target gene in response to NO_3^-; blue edges represent protein–DNA interactions from TFs that are disengaged from the target gene in response to NO_3^-; gray edges represent protein–DNA interactions from TFs bound at all tested conditions; and black thick edges represent TF–TF interactions. The size of the triangle is proportional to the number of targets bound by the TF.

(B) Phenotypes of the Col-0, and BEE2-, HB23-, and AGL5-overexpressing plants grown on medium plates under limiting nitrate conditions.

(C) Plant growth of *BEE*, *HB23*, and *AGL15* overexpressor lines is enhanced compared with wild-type plants under limiting nitrate conditions (0.1 mM KNO_3).

(D) Primary root growth of *BEE*, *HB23*, and *AGL15* overexpressor lines is enhanced compared with wild-type plants under limiting nitrate conditions (0.1 mM KNO_3).

(C and D) All values plotted correspond to the means of three independent biological replicates ± standard deviations. Different letters indicate that means values differ significantly between genotypes (*t* test, $p < 0.05$).

2014), NLP7-*NIA1*, and NLP7-*NIR* (Marchive et al., 2013) (Supplemental Tables 6 and 7). Altogether, these comparisons indicate that our footprinting approach recapitulates validated connections between TF and targets and provides reliable information to identify novel regulatory interactions.

To gain further insight into the transcriptional wiring implicated in root responses to NO_3^- and identify new candidate TFs, we generated a core transcriptional network with TFs that are recruited or disengaged in response to nitrate at promoter regions of nitrate-regulated genes. Most of these TFs also showed stable footprinting patterns, and these interactions were included as well (Figure 5A, Supplemental Table 6). The resulting network comprised 373 edges connecting 52 TF nodes with 108 target nodes regulated by NO_3^- (Figure 5A). Our analysis resulted in a highly connected network in which TFs (triangles) are arranged into four tiers according to the number of target genes (outdegree). The size of the TFs in this network is proportional to the outdegree. A recent single-cell RNA-seq approach reveals cell-specific patterns of gene expression in roots (Denyer et al., 2019). By integrating these data in our network, we found most of the TFs, whose expression was detected in this study, are expressed in at least

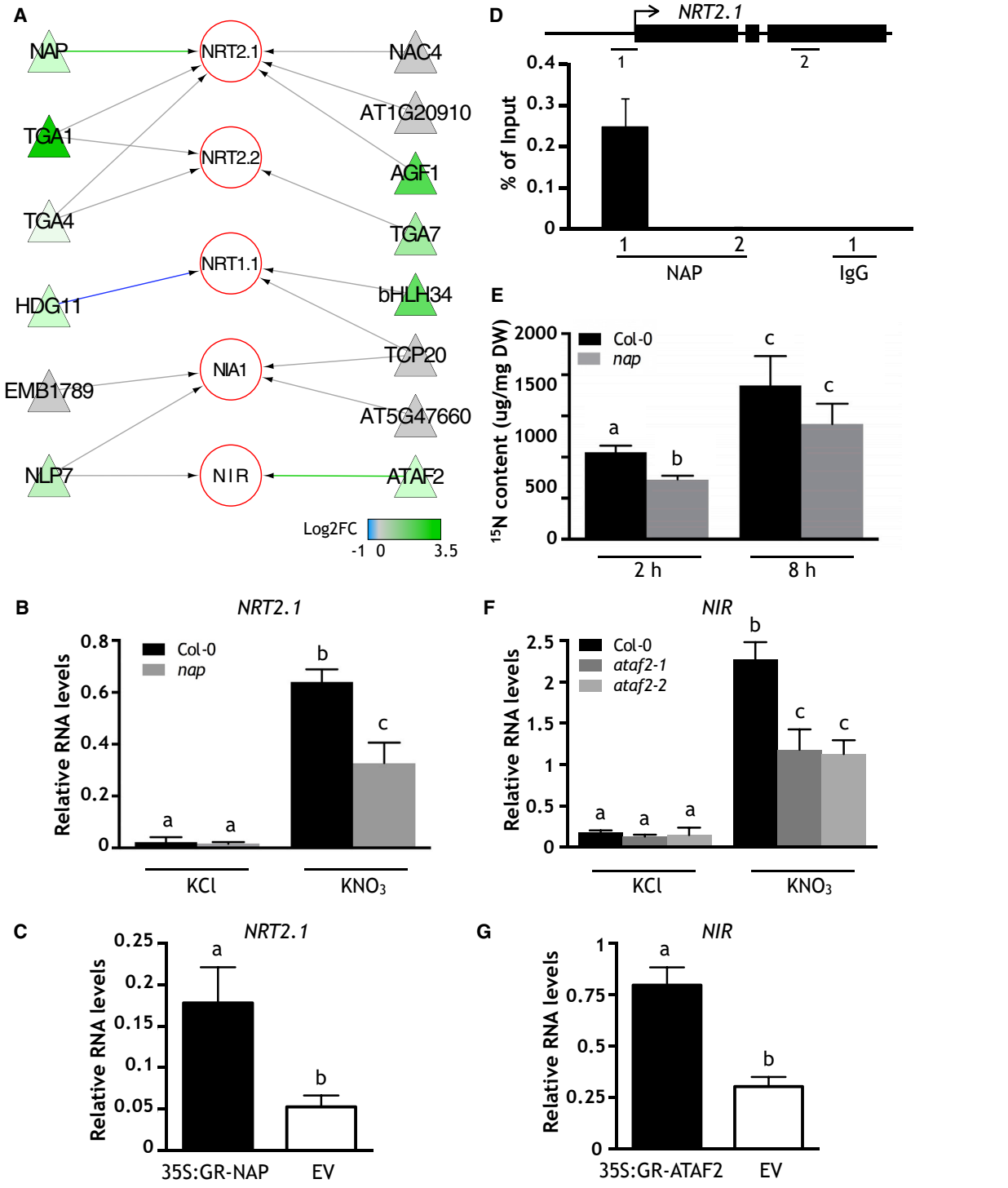

Figure 6. Subnetwork with Prototypical NO_3^--Responsive Genes Reveals NAP Is an Activator of NO_3^- Transport, and ATAF2 Induces the Expression of *NIR*.

(A) Color of triangles represents TF expression levels in response to NO_3^-, according to our RNA-seq experiments. Green edges represent protein–DNA interactions from TFs that are recruited to the target gene in response to NO_3^-; blue edges represent protein–DNA interactions from TFs that are disengaged from the target gene in response to NO_3^-; gray edges represent protein–DNA interactions from TFs bound at all tested conditions.

(B) NAP is required for the nitrate-dependent upregulation of *NRT2.1* mRNA levels.

(C) TARGET assay reveals NAP directly regulates the expression of *NRT2.1*.

(legend continued on next page)

one cell type in roots (Supplemental Figure 11). This result suggests the TFs act in multiple cell layers. We found 20 TFs regulated by NO_3^- and 32 TFs that are not regulated by NO_3^- under our experimental conditions (Figure 5A). Interestingly, the upper tier in the network is composed of new TFs whose expression is not regulated by NO_3^-. The two intermediate tiers are composed of 30 TFs, including several known nitrate regulatory factors such as TGA1, TGA4, and CCA1. The lower tier is composed of 14 NO_3^--responsive TFs, including the known regulator NLP7. Consistent with a signaling network with primary and secondary responses, most TF–TF interactions in this network are directed from TFs in upper tiers that are not regulated by nitrate. These TFs would control expression of NO_3^--responsive TFs in lower tiers, including some of the TFs described in the literature (e.g., NLP7). This network proposes a mechanism for nitrate signal amplification from TFs to TFs to known targets in metabolism and other processes.

Newly Identified TFs Play a Role in NO_3^- Responses

Perturbation of TFs involved in gene expression in response to nitrate alters plant growth (Guan et al., 2014; Zhong et al., 2015; Yu et al., 2016). With the hypothesis that TFs in our network regulate nitrate responses, we examined plant growth in inducible overexpression lines (Coego et al., 2014) for three TFs that belong to different levels of hierarchy. We evaluated the role of HB23 and AGL15, which are in the upper layer of our regulatory network, and BEE2, which is in the lower layer. We used two independent lines per gene and Col-0 plants transformed with the empty vector used to generate the transgenic TRANSPLANTA lines as a control (Coego et al., 2014). We found that overexpression of the three TFs led to an increase in plant growth and primary root growth under limiting NO_3^- conditions compared with Col-0 plants (Figure 5B–5D). Under sufficient NO_3^- conditions, the biomass and primary root growth of overexpressor lines was similar to Col-0 plants (Supplemental Figure 12). These results indicate HB3, AGL15, and BEE2 have a role in plant growth in response to NO_3^- availability.

NAP and ATAF2 Regulate Important Steps in NO_3^- Uptake or Reduction

A primary function of nitrate regulatory networks is NO_3^- uptake and NO_3^- reduction genes. These are key steps in the control mechanisms that plants use to maximize nitrogen-use efficiency. They have, for a long time, been the focus of research seeking to understand molecular mechanism underlying NO_3^- responses (reviewed in Krapp et al., 2014; Krouk et al., 2010a; Undurraga et al., 2017; Vidal et al., 2015). To provide additional insight into these important aspects of nitrate metabolism, we selected a subnetwork with TFs bound to prototypical NO_3^--responsive genes, including *NRT1.1*, *NRT2.1*, *NRT2.2*, *NIA1*, and *NIR* (Figure 6A). This network captured validated interactions by ChIP, including TGA1-*NRT2.1* and TGA1-*NRT2.2* (Alvarez et al., 2014), NLP7-*NIA1* and NLP7-*NIR* (Marchive et al., 2013), TCP20-*NIA1* and TCP20-*NRT1.1* (Guan et al., 2014) (Supplemental Table 7). Most targets in this network were regulated by multiple TFs. *NRT2.1* was the target of many TFs, likely reflecting the fine transcriptional control of this important gene in nitrate uptake. We found that NAP and ATAF2 are both recruited to the promoter regions of *NRT2.1* and *NIR*, respectively, in response to NO_3^- treatments. These results indicate that NAP and ATAF2 are positive regulators of the expression of *NRT2.1* and *NIR* genes.

NAP has been previously characterized as a transcriptional activator (Yang et al., 2014). To test whether NAP has a role in the activation of gene expression in response to NO_3^- treatments, we first measured mRNA levels of *NRT2.1* by qRT–PCR after NO_3^- treatments in wild type and a *nap* mutant line (Sakuraba et al., 2015). As shown in Figure 6B, *NRT2.1* gene expression was induced by nitrate treatments in wild-type plants. However, nitrate induction of *NRT2.1* was significantly dampened (~50%) in the *nap* mutant. In a complementary approach, we used the cell-based TARGET assay to test whether NAP directly regulates the expression of *NRT2.1*. To perform the TARGET assay, we transiently overexpressed NAP in root protoplasts as an NAP glucocorticoid receptor fusion protein (35S:GR-NAP). Transfected protoplasts expressing GR-NAP were sequentially treated with KNO_3, cycloheximide (CHX), and dexamethasone (DEX). DEX treatment induces nuclear import of the GR-TF fusion protein (Bargmann et al., 2013; Para et al., 2014). Pre-treatment with CHX blocks downstream regulation of secondary TF targets (Bargmann et al., 2013; Para et al., 2014). Thus, direct TF targets can be identified as those that respond transcriptionally to DEX-induced TF nuclear import in the presence of CHX. As expected, *NAP* transcript levels were higher in 35S:GR-NAP transfected protoplast compared with control protoplasts transfected with an empty vector (EV) lacking the TF (Supplemental Figure 13A). We found significantly higher *NRT2.1* expression levels in protoplast overexpressing NAP compared with the EV control (Figure 6C). This result indicates NAP directly activates the expression of *NRT2.1*. We used ChIP assays with an NAP-specific antibody and a non-specific IgG as a negative control to further validate NAP-*NRT2.1* direct interaction. Immunoprecipitated DNA was amplified by qPCR using primers designed to span the region where the NAP footprint was detected in the promoter of *NRT2.1* (Figure 6D). We found NAP was able to bind specifically to the *NRT2.1* promoter region because no significant signal was observed when we used primers

(D) NAP binds *in vivo* specifically to *NRT2.1* promoter. ChIP assays using antibodies against NAP and a non-specific IgG as a negative control. Immunoprecipitated DNA was quantified by qPCR with primers that encompass the NAP footprint in the *NRT2.1* promoter (fragment indicated as "1") and for a control region in the coding sequence (fragment indicated as "2"). Results were normalized to the input DNA.
(E) ^{15}N content is affected in *nap* mutant plants. $^{15}NO_3^-$ content was measured after treatments with 250 μm for 2 and 8 h and normalized by the plant dry weight.
(F) ATAF2 is required for the nitrate-dependent upregulation of *NIR* mRNA levels.
(G) TARGET assay reveals ATAF2 directly regulates the expression of *NIR*. Empty vector (EV) lacking the TF was used for control protoplasts. The *clathrin adaptor complexes medium subunit family protein* gene (At4g24550) was used for normalization of RT–qPCR.
(B–G) All values plotted correspond to the means of three independent biological replicates ± standard deviations. Different letters indicate statistically different means (*t* test, $p < 0.05$).

designed against the *NRT2.1* coding sequence (Figure 6D). No significant signal was detected in the immunoprecipitation with the non-specific IgG. We found that NO_3^- content is affected in *nap* mutants compared with the wild-type plants, consistent with misregulation of *NRT2.1* in the *nap* mutant (Figure 6E). These results indicate that NAP is a direct activator of *NRT2.1* expression in response to NO_3^- and a novel positive regulator of NO_3^- uptake in roots.

Our network analysis also indicated ATAF2 is a positive regulator of *NIR* expression (Figure 6A). To further corroborate this interaction, we measured mRNA levels of *NIR* by qRT–PCR after NO_3^- treatments in wild type and two *ataf2* mutant lines (Peng et al., 2015). We found *NIR* expression was induced by nitrate treatments in the wild-type plants. However, nitrate induction of *NIR* was significantly lower in both *ataf2* mutant alleles (Figure 6F). This result indicates ATAF2 positively regulates the expression of *NIR* in response to nitrate treatments. Using the TARGET assay, we found significantly higher levels of *ATAF2* and *NIR* expression in protoplasts overexpressing ATAF2 compared with the EV control (Figure 6G; Supplemental Figure 13B). This result indicates ATAF2 directly activates *NIR* expression.

DISCUSSION

We found NO_3^- produces a rapid increase in RNPII occupancy that is associated with both early and late changes in transcript accumulation. We found that the overall chromatin accessibility patterns do not change in the promoter of transcriptionally regulated genes up to 2 h after NO_3^- treatments. However, differential TF footprints by NO_3^- localized within "open" chromatin regions correlate with transcriptional activation in response to this nutrient signal. These results indicate that preexisting patterns of chromatin accessibility are determinants for the rapid nitrate response that is mediated by binding of specific TFs that modulate transcription of target genes. Using genomic footprinting by DNase-seq and ChIP assays in mouse, John et al. (2011) demonstrated that a high proportion of *de novo* genomic binding by the glucocorticoid receptor, a ligand-activated TF, is targeted to preexisting regions of accessible chromatin. This mechanism would be consistent with rapid changes in gene expression without large changes in chromatin remodeling. Recently, regulatory DNA landscape dynamics were analyzed during photomorphogenesis (Sullivan et al., 2014). In seedlings, light triggers photomorphogenesis, a fundamental and irreversible reshaping of plant form and metabolism to optimize photosynthesis. Underlying this transition is a wave of transcriptional re-programming and alteration in chromatin compaction (van Zanten et al., 2012). Sullivan et al. (2014) found changes in chromatin accessibility after 3 and 24 h of light treatments. However, they only found minor changes in chromatin accessibility after 30 min of light exposure. These findings together with our data suggest that large chromatin changes would be required for major and perhaps irreversible changes in plant form and functions at the organism level, but not for rapid changes in response to an environmental stimulus in specific organs.

The chromatin factor high nitrogen-insensitive 9 (HNI9) was shown to be involved in response to a high N provision in *Arabidopsis* (Widiez et al., 2011). Plants grown in an excessive N environment express a set of genes involved in detoxification of reactive oxygen species (ROS) that maintain ROS at physiological levels (Bellegarde et al., 2019). HNI9 is an important regulator of this response through influencing the histone modification state of genes, mainly at maintaining H3K4me3 levels
(Bellegarde et al., 2019). This study is an example of how a long-term high N provision has an impact on the chromatin state that differs from short nitrate treatments having a marginal effect on chromatin accessibility.

Recently, the cell-based TARGET assay was scaled up to identify the direct targets of 33 TFs regulated by N at early time points (Brooks et al., 2019). The TARGET assay can validate direct TF–target interactions based solely on TF-induced changes in gene expression (Bargmann et al., 2013; Brooks et al., 2019). Interestingly, the authors found each TF can act in a dual mode (to induce or repress) depending on the *cis*-motif context of the target gene. This dual TF action could operate via direct binding to a *cis*-element or indirectly via a partner TF_2 binding (Brooks et al., 2019).

Our data established the relative hierarchical contribution of known TFs validated in previous studies and new TFs based on direct binding to DNA. Interestingly, we found that the higher tier is composed of TFs that have not been implicated in nitrate responses thus far. These TFs are not regulated by nitrate at the level of gene expression, which has been an important criterion to find many of the regulatory factors to date, including the TARGET study that validate 33 TFs (Brooks et al., 2019). We found that most of the TF–TF interactions in our network stem from TFs that are not regulated by nitrate in upper tiers and target NO_3^--responsive TFs in lower tiers. These results are consistent with a hierarchical transcriptional regulatory network, which amplifies the NO_3^- signal to affect many biological processes. Nitrate transporters *NRT1.1*, *NRT2.1*, and *NRT2.2* and nitrate metabolic genes *NIA1* and *NIR* are convergent targets of many of the known TFs (Castaings et al., 2009; Marchive et al., 2013; Alvarez et al., 2014; Guan et al., 2014). Consistent with this, we found that genes involved in NO_3^- transport and NO_3^- reduction are targeted by multiple TFs. Previous studies have shown that a single TF does not explain the full induction of prototypical NO_3^--responsive genes such us *NRT2.1*, *NRT2.2*, *NIA1*, and *NIR* (Castaings et al., 2009; Alvarez et al., 2014; Guan et al., 2014). Indeed, protein–protein interactions between TFs (e.g., NLP7-TCP20 and NRG2-NLP7) have been found to be important for gene expression of prototypical NO_3^--responsive genes (Xu et al., 2016; Guan et al., 2017). We identified ATAF2 and NAP as new TFs that positively regulate the expression of *NIR* and *NRT2.1* in response to nitrate, respectively. Recently, TF–TF interactions were explored and described using HaloTag protein arrays (Yazaki et al., 2016). This report revealed that NAP interacts with TGA1, which is also known to be involved in nitrate induction of *NRT2.1* (Alvarez et al., 2014). We detected NAP and TGA1 footprints in the promoter of *NRT2.1*, suggesting that NAP–TGA1 interaction has a functional importance for *NRT2.1* expression. Further characterization is necessary to address the role of NAP–TGA1 interaction in the nitrate response.

Our findings highlight ATAF2, NAP, and other components of the intricate regulatory network that participate in fine and robust control of genes that are targets of N-nutrient signals. This network is rich in new targets for biotechnological applications that may have an impact on nitrate uptake, reduction, N assimilation, and use. Thus, it represents a valuable resource for future fundamental and applied research for the plant community.

METHODS

Plant Materials and Growth Conditions

We grew approximately 1500 *Arabidopsis thaliana* Col-0 seedlings in 200-ml hydroponic cultures under long-day (16-h light/8-h dark) conditions at 22°C in plant growth incubators (Percival Scientific) using MS-modified basal salt media without N (Phytotechnology Laboratories), supplemented with 0.5 mM ammonium succinate and 3 mM sucrose. Plants were grown for 2 weeks and treated for the indicated period of time at the beginning of the light cycle on day 15 with 5 mM NO_3^- or with 5 mM KCl as a control.

DNA-Seq

Plants were grown hydroponically as mentioned above and collected at time 0 or treated with 5 mM KNO_3 or 5 mM KCl as a control for 12 min or 2 h. We generated a high-resolution map of DHSs in *A. thaliana* root organs, including untreated controls (time 0), KCl treatments and KNO_3 treatments, and two naked DNA controls (Supplemental Table 3). DNase-seq library construction followed published protocols with only minor modifications (Boyle et al., 2008b). Briefly, roots were collected and ground into a fine powder in liquid nitrogen. The resulting powder was suspended in nuclear isolation buffer (20 mM Tris-HCl, 50 mM EDTA, 5 mM spermidine, 0.15 mM spermine, 0.1% mercaptoethanol, 40% glycerol at pH 7.5) and followed the standard protocol for nuclei isolation. The prepared nuclei pellet was suspended in RSB buffer (10 mM Tris at pH 7.4, 10 mM NaCl, 3 mM $MgCl_2$) for DNase I (Roche) digestion with increasing concentrations (0–4 units) for 10 min at 37°C. The degree of DNase I digestion was assessed by pulsed-field gel electrophoresis (PFGE; 20–60 switch time, 18 h, 6 V/cm; Bio-Rad). High-molecular-weight (HMW) DNA after DNase I digestion was isolated and blunt ended with T4 DNA polymerase. Biotinylated adaptor I (5′ Bio ACA GGT TCA GAG TTC TAC AGT CCG AC and 5′ P-GTC GGA CTG TAG AAC TCT GAA C) was ligated to the DNA molecules. Dynal M-280 beads (Invitrogen) were used for enriching DNase I–digested DNA ends after MmeI digestion. Adaptor II (5′ P-TCG TAT GCC GTC TTC TGC TTG and 5′-CAA GCA GAA GAC GGC ATA CGA NN) was then ligated to the MmeI-treated ends. The DNA sample was amplified by PCR using linker-specific primers (5′-CAA GCA GAA GAC GGC ATA CGA and 5′-AAT GAT ACG GCG ACC ACC GAC AGG TTC AGA GTT CTA CAG TCC GA) and purified by PAGE for isolation of DNA fragments 90 bp in size. The final Illumina sequencing was performed using a primer specific to linker I (5′-CCA CCG ACA GGT TCA GAG TTC TAC AGT CCG AC) on the HiSeq 2000 platform (Illumina, San Diego, CA). For naked DNA control libraries, 5 μg of purified deproteinized DNA was suspended in 160 μl of RSB buffer by aliquoting 20 μl into each of eight tubes. An equal volume of RSB buffer with DNase I at increasing concentrations (0–4 units) for 2 min at 37°C was added to the DNA. Two microliters of digested material from each treatment was loaded on a 2% TAE agarose gel and run for 1 h at 100 V to assess the degree of digestion. Treatments with moderate levels of digestion (average fragment size >400 bp) were pooled for library preparations. Library construction was performed as for the DNA-seq libraries as mentioned above.

Chromatin Immunoprecipitation Assays, Library Generation, and Sequencing

ChIP assays were performed as previously described (Saleh et al., 2008). Briefly, plants grown as indicated above were treated with 5 mm KNO_3 or 5 mm KCl as a control for 12 min. Roots were collected after the treatments and immediately fixed in 1% formaldehyde for 15 min under vacuum at 25°C. Isolated chromatin was sonicated with a Bioruptor sonicator (Diagenode, Belgium). The Bioruptor settings were as follows: 25 cycles of 0.5 min on, 0.5 min off, with 5 min rests between every five cycles. An aliquot of sheared chromatin was removed to serve as a control (input). Experiments were performed in two independent biological replicates. A commercial antibody against the CTD of RNPII (Ab817, Abcam) was used in ChIP experiments. Resulting ChIP DNA pooled from two ChIP reactions described above was used to generate a sequencing library using the TruSeq DNA Sample Prep Kit (Illumina, San Diego, CA). We also sequenced input DNA form each condition as a control. The Illumina HiScanSQ (Illumina, San Diego, CA) was used to sequence the single-read ChIP-seq and input libraries as per the manufacturer's instructions for 100 bp.

ChIP-Seq Data Analysis

Bowtie2 software (Langmead and Salzberg, 2012) was used to align the reads to the Col-0 reference genome TAIR10 (ftp://ftp.arabidopsis.org/). Only the reads mapped to a unique position of the *A. thaliana* genome were used for further analysis. To evaluate differential RNPII occupancy on the genes, we used sequence counts in regions spanning 500-bp upstream of the TSS, gene body and 500-bp downstream of the TTS of protein coding genes as input for the DESeq2 package (Love et al., 2014) available from Bioconductor (http://www.bioconductor.org). Differential RNPII occupancy was calculated with two independent biological replicates in roots treated with KNO_3 or KCl for 12 min (1.5-fold change in occupancy level, $p < 0.05$).

DNase-Seq Data Analysis

DNase-seq reads were aligned to the *Arabidopsis* genome (TAIR10) with no mismatches allowed using Bowtie2 (Langmead and Salzberg, 2012). Only sequence reads mapped to a unique position were used for further analysis. We used F-seq (Boyle et al., 2008b) to identify DHSs with a 300-bp bandwidth. To estimate the FDR, we generated 10 random datasets that contained the same read number as the DNase-seq dataset. FDR was calculated as the ratio of the number of DHSs identified based on random datasets with F-seq to the number of DHSs from the DNase-seq data. A threshold was set in F-seq to control the FDR <0.01. We identified between 30 030 and 36 395 DHSs per library with a high reproducibility between biological replicates (Supplemental Table 3).

SPOT score for each library was calculated with the hotspot tool as previously described (John et al., 2011; Alexandre et al., 2018). To calculate the correlation between replicates, we generated a merged DHS between replicates. The log10(cut counts per 150 bp window) was calculated for each replicate within the merged DHS. The values obtained were used to calculate the correlation (Supplemental Table 3) and used for scatter plots (Supplemental Figure 5).

To identify differential DHSs between treatments, the DHSs of all conditions to be compared were merged to create a "union" DHS. Per base DNaseI cleavage DNase-seq reads mapping within each merged DHS were counted with the Rsubread package (Liao et al., 2019) for each library. We used these counts as input for the DESeq2 package (Love et al., 2014). Differential DHSs was calculated with two independent biological replicates in roots treated with KNO3 or KCl for 12 min; 12 min of KNO_3 treatments or time 0; 2 h of KNO_3 treatments or 2 h of KCl treatments (log2 fold change >1 in DHS level, $p < 0.05$; Supplemental Table 4). DESeq2 analysis was repeated with the counts from DNase-seq libraries that were subsampled to the number of reads of the library with the lower read depth as input. .BAM files were randomly subsampled using the SAMtools package (Li et al., 2009).

Footprinting Data Analysis

Positional weight matrices (PWM) of TF motifs from three databases were collected: (i) DAP-seq (O'Malley et al., 2016), (ii) CIS-BP protein binding

microarrays (PBMs) (Weirauch et al., 2014) (only PWM with direct experimental evidence), and (iii) from an additional source of PBM (Franco-Zorrilla et al., 2014). The collected PWMs were used to call TF motif matches in the *A. thaliana* genome using the MEME/FIMO suite tool (Grant et al., 2011). To identify footprints resulting from protein binding, we used the TF motif as the center to align sequences within DHSs on each DNase-seq library. We then counted the numbers of DNase I cut at each nucleotide of the TF motif and 100 bp around the motif based on the numbers of DNase-seq reads. We used CENTIPEDE to measure the level of "protection" of the TF motif to the DNaseI cut and calculated a footprinting score (Pique-Regi et al., 2011) to determine whether a footprint can be called within a specific locus. The CENTIPEDE approach allows predicting TF–DNA binding using the spatial pattern distribution of reads from DNase-seq data and the DNA sequence of TF motifs at the binding site (Gusmao et al., 2016). Only those TF footprints with a posterior probability = 1 were retained (Pique-Regi et al., 2011). To avoid footprint calling due to the molecular structure of DNA itself, we used two naked DNA controls; a sample stripped of proteins was also digested with DNaseI and sequenced. Finally, only those footprints detected in both biological replicates and not detected in any of the naked DNA libraries were called. We define footprints as "TF recruited by NO_3^-" (Figure 3) when detected in both DNase-seq replicates of KNO_3 treatments, and none of the DNase-seq replicates at time 0 or KCl treatments. We define footprints as "TF disengaged by NO_3^-" when detected in both DNase-seq replicates of time 0 and KCl treatments and none of the DNase-seq replicates of KNO_3 treatments. The defined TF footprint was associated with the respective TF according to the three TF motif databases mentioned above. A TF–target gene interaction was defined when a TF footprint overlapped within 1000 bp upstream of the TSS of the target gene.

Total RNA Extraction, PolyA Selection, and mRNA-Seq Library Generation

RNA was isolated from whole roots with Trizol reagent according to the manufacturer's instructions (Invitrogen, now Life Technologies, http://www.lifetechnologies.com). To perform RNA-seq experiments, roots were harvested for RNA isolation after 12, 20, 60, and 120 min of KNO_3 or KCl exposure. At least 30 μg of total RNA was subject to polyA selection using the Poly(A) Purist MAG Kit (Ambion, cat. no. AM1922). 50–100 ng of polyA RNA was used in a strand-specific library preparation as per the SOLiD Total RNA-Seq Kit protocol (Invitrogen, cat. no. 4445374), and AMPure XP beads (Agencourt, cat. no. A63881) were used for purification of cDNA and amplified DNA. Libraries were sequenced for 50 bp on the SOLiD4 platform (Life Technologies, Carlsbad, CA).

mRNA-Seq Analysis

The Bowtie software (Langmead and Salzberg, 2012) was used to align the reads to the Col-0 reference genome TAIR10 (ftp://ftp.arabidopsis.org/). Only the reads mapped to a unique position of the *A. thaliana* genome were used for further analysis. To evaluate differential gene expression between KNO_3- and KCl-treated samples, we used sequence counts corresponding to protein coding genes elements as input for the DESeq2 package (Love et al., 2014) available from Bioconductor (http://www.bioconductor.org).

Network Generation and Visualization

To build networks, an edge was created when a footprinted motif of a source TF overlapped a target gene, including 1000 bp upstream of the target gene's TSS. "Target genes" are genes showing both an increase in RNPII occupancy and an increase in transcript levels in response to NO_3^-. We used Cytoscape to visualize the resulting network in which genes are represented as nodes connected by edges that represent TF–DNA interactions found by the footprinting analysis. For our matrix with TF–target interactions (Supplemental Figure 5), TF–target interactions (edges) were generated based on nitrate-modulated footprints and footprints detected regardless of the experimental conditions. TFs in Figure 5A exhibit at least one nitrate-modulated footprint in the promoter of target genes. Most of these TFs also showed footprints detected in all conditions, and these interactions were included as well. To design the network of Figure 5A, we used a hierarchical layout available in Cytoscape tools to arrange the TFs according to outdegree (number of target genes) from high (upper layers) to low (lower layers).

Plant Material and Growth Conditions for TRANSPLANTA Overexpressing Lines

We used two independent T3 homozygous *Arabidopsis thaliana* inducible lines of the identified TFs BEE2, HB23, and AGL15 from the TRANSPLANTA collection (Coego et al., 2014). Col-0 plants transformed with the EV used to generate the transgenic TRANSPLANTA lines were used as a control. Seeds were surfaced sterilized, stratified at 4°C for 2 days, and grown for 11 days on vertical plates in a chamber at 22°C/18°C under long-day (16 h/8 h, light/dark) conditions. MS-modified basal salt medium without N (M531, Phytotechnology Laboratories) containing 1% (w/v) sucrose, 0.8% (w/v) plant agar, and 10 mM b-stradiol, and supplemented with 10 mM KNO_3, 5 mM KNO_3, or 0.1 mM KNO_3. To compensate the potassium balance in the N-limiting medium, KCl in its appropriate molarity was added. Three replicates per genotype and condition were performed, and at least 12 seeds were used in every replicate. Plates were photographed and the fresh weight of the plants was measured.

RNA Isolation and qRT–PCR

Col-0 and *nap* (Sakuraba et al., 2015) plants were grown under the same experimental conditions described above. Plants were treated for 2 h on day 15 with 5 mm KNO_3 or with 5 mm KCl as a control. RNA was isolated from whole roots with Trizol reagent according to the manufacturer's instructions (Invitrogen, now Life Technologies, http://www.lifetechnologies.com). cDNA synthesis was carried out using Improm-II reverse transcriptase according to the manufacturer's instructions (Promega, http://www.promega.com). qRT–PCR was carried out using the Brilliant SYBR Green QPCR reagents on a Stratagene MX3000P qPCR system (Stratagene, now Agilent, http://www.genomics.agilent.com). The RNA levels were normalized relative to *clathrin adaptor complexes medium subunit family protein* (At4g24550). Amplification was performed using the following set of primers: *NRT2.1* (forward, 5′-ACT TGA AGC TCC ACA CAG CA-3′; reverse, 5′-ATC CAC AAC GTC CAC AAC CT-3′) and *At4g24550* (forward 5′-AAT ACG CGC TGA GTT CCC TT-3′; reverse, 5′-AGC ACC GGG TTC TAA CTC-3′).

TARGET Assays

For the TARGET assay, NAP and ATAF2 were TOPO cloned into pENTR (Invitrogen) from cDNA or isolated from the *Arabidopsis* TF collection (Pruneda-Paz et al., 2014). TFs were then transferred to the pBeaconRFP_GR plasmid (Bargmann et al., 2013) or a GFP version of the same plasmid (pBeaconGFP_GR) by Gateway (Invitrogen) cloning. Root protoplasts from *Arabidopsis* Col-0 plants were prepared, transfected, and sorted as previously described (Bargmann et al., 2013; Para et al., 2014). For each TF and the EV construct, 3×10^6 cells were transformed separately, and after washing, a single TF in the RFP vector and a single TF in a GFP vector were combined in three replicate wells of a 24-well plate. After overnight incubation, each pool of transformed root protoplasts was treated sequentially with 5 mM KNO_3 for 100 min and 35 μM CHX for 20 min before a 10 μM DEX treatment to induce TF nuclear entry. Transformed cells were sorted by fluorescence-activated cell sorting into GFP- and RFP-expressing populations 3 h after DEX-induced TF nuclear import. Cells overexpressing the TF or EV were collected in triplicate, and RNA was extracted using the RNeasy Plant Mini kit (QIAGEN, 74904). cDNA synthesis was carried out using the Improm-II reverse transcriptase according to the manufacturer's instructions (Promega, http://www.promega.com). qRT–PCR was carried out using the Brilliant SYBR Green QPCR reagents on a Stratagene MX3000P qPCR system (Stratagene, now Agilent, http://www.genomics.agilent.com). The RNA levels were normalized relative to *clathrin adaptor complexes medium subunit family protein* (At4g24550).

Amplification was performed using the following set of primers: *NRT2.1* (forward, 5′-ACT TGA AGC TCC ACA CAG CA-3′; reverse, 5′-ATC CAC AAC GTC CAC AAC CT-3′); *NIR* (forward, 5′-ACA CTT GCG GAC AAG TCC AAG TAG-3′; reverse, 5′-TCT CCG ATA TGC GAG TCA CTT CCT-3′); *NAP* (forward, 5′-ACG TGT TCG CTG GCT CAT TT -3′; reverse, 5′-CCG AAC CAA CTA GAC TCC GAA TCA-3′); ATAF2 (forward, 5′-GCC TGA GCA GAA ACC ATT CTT G-3′; reverse, 5′-AAG AGC CAG GGA TGA GTT GAG A-3′); and *At4g24550* (forward 5′-AAT ACG CGC TGA GTT CCC TT-3′; reverse, 5′-AGC ACC GGG TTC TAA CTC-3′).

ChIP–PCR Assays

Col-0 plants were grown under the same experimental conditions described above. Plants were treated for 12 min on day 15 with 5 mm KNO_3. ChIP assays were performed as described above. A small aliquot of sheared chromatin was removed to serve as a positive control of PCR amplification (input). The diluted chromatin was used for immunoprecipitation with the NAP antibody (Abmart, X3-O49255), and an unspecific IgG was used as a negative control. Immunoprecipitated DNA was amplified by PCR using the following sets of primers: *NRT2.1* promoter (forward, 5′-TTG CGG CGA AAA TGG ATT CCT C-3′; reverse, 5′-ATA GGG TTC CTA GCC AGT GTT GAC-3′) and *NRT2.1 CDS* (forward, 5′-ACT TGA AGC TCC ACA CAG CA-3′; reverse, 5′-ATC CAC AAC GTC CAC AAC CT-3′).

Net Nitrate Uptake Experiments

Col-0 and *nap* plants were grown under the same experimental conditions described above. Net NO_3^- uptake was measured by treating plants at dawn on day 15 with 250 μm $^{15}NO_3^-$ (atom% ^{15}N: 10%) for 2 and 8 h. After the indicated time periods, roots were washed for 1 min in 0.1 mm $CaSO_4$ and were separated from shoots. Roots were dried at 70°C for 48 h and were analyzed for total $^{15}NO_3^-$ contents using an ANCA-MS system (Europa Scientific, http://www.europascience.com). Net uptake of $^{15}NO_3^-$ for each genotype was calculated from the total ^{15}N content of roots.

ACCESSION NUMBERS

All sequence data from this project have been deposited in NCBI's GEO database (GEO: PRJNA563066).

SUPPLEMENTAL INFORMATION

Supplemental Information is available at *Molecular Plant Online*.

FUNDING

This work is funded by Instituto Milenio iBio - Iniciativa Científica Milenio MINECON, Chile; by grants from the Fondo de Desarrollo de Areas Prioritarias (FONDAP) Center for Genome Regulation (15090007), Chile; and Fondo Nacional de Desarrollo Científico y Tecnológico (FONDECYT) (1180759), Chile; to R.A.G. J.M.A. is supported by postdoctoral grant FONDECYT (3140336), Chile.J.J. is funded by grant MCB-1412948 from the National Science Foundation, United States; and J.M. by funding from the Instituto Nacional de Investigación y Tecnología Agraria y Alimentaria (INIA), Spain (RTA2015-00014-c02-01). We also want to acknowledge the "Severo Ochoa Program for Centers of Excellence in R&D" from the Agencia Estatal de Investigación of Spain (SEV-2016-0672 (2017–2021)) for supporting the scientific services used in this work.

AUTHOR CONTRIBUTIONS

The experimental plan was designed by J.M.A. F.J.H.., J.J., J.M., J.V-C., and R.A.G. Laboratory experiments were performed by J.M.A, D.G., V.A., J.A.O., and L.C.; genomic analysis was performed by J.M.A, T.C.M., and T.Z.; the manuscript was written by J.M.A., and R.A.G. The authors declare no competing interests.

ACKNOWLEDGMENTS

We thank Dr. Gloria Coruzzi, who allowed J.M.A. to perform the TARGET experiment in her lab. We thank Dr. Matthew D. Brooks and Angelo V. Pasquino for their help with the TARGET experiment. We thank Dr. Michael Neff who kindly donated seeds from the *ataf2-1* and *ataf2-2* mutants. No conflict of interest declared.

Received: April 12, 2019
Revised: August 27, 2019
Accepted: September 5, 2019
Published: September 14, 2019

REFERENCES

Alexandre, C.M., Urton, J.R., Jean-Baptiste, K., Huddleston, J., Dorrity, M.W., Cuperus, J.T., Sullivan, A.M., Bemm, F., Jolic, D., Arsovski, A.A., et al. (2018). Complex relationships between chromatin accessibility, sequence divergence, and gene expression in *Arabidopsis thaliana*. Mol. Biol. Evol. **35**:837–854.

Alvarez, J.M., Vidal, E.A., and Gutierrez, R.A. (2012). Integration of local and systemic signaling pathways for plant N responses. Curr. Opin. Plant Biol. **15**:185–191.

Alvarez, J.M., Riveras, E., Vidal, E.A., Gras, D.E., Contreras-López, O., Tamayo, K.P., Aceituno, F., Gómez, I., Ruffel, S., and Lejay, L. (2014). Systems approach identifies TGA1 and TGA4 transcription factors as important regulatory components of the nitrate response of *Arabidopsis thaliana* roots. Plant J. **80**:1–13.

Bargmann, B.O., Marshall-Colon, A., Efroni, I., Ruffel, S., Birnbaum, K.D., Coruzzi, G.M., and Krouk, G. (2013). TARGET: a transient transformation system for genome-wide transcription factor target discovery. Mol. Plant **6**:978–980.

Bellegarde, F., Maghiaoui, A., Boucherez, J., Krouk, G., Lejay, L., Bach, L., Gojon, A., and Martin, A. (2019). The chromatin factor HNI9 and ELONGATED HYPOCOTYL5 maintain ROS homeostasis under high nitrogen provision. Plant Physiol. **180**:582–592.

Boyle, A.P., Davis, S., Shulha, H.P., Meltzer, P., Margulies, E.H., Weng, Z., Furey, T.S., and Crawford, G.E. (2008a). High-resolution mapping and characterization of open chromatin across the genome. Cell **132**:311–322.

Boyle, A.P., Guinney, J., Crawford, G.E., and Furey, T.S. (2008b). F-Seq: a feature density estimator for high-throughput sequence tags. Bioinformatics **24**:2537–2538.

Boyle, A.P., Song, L., Lee, B.K., London, D., Keefe, D., Birney, E., Iyer, V.R., Crawford, G.E., and Furey, T.S. (2011). High-resolution genome-wide in vivo footprinting of diverse transcription factors in human cells. Genome Res. **21**:456–464.

Brooks, M.D., Cirrone, J., Pasquino, A.V., Alvarez, J.M., Swift, J., Mittal, S., Juang, C.L., Varala, K., Gutierrez, R.A., Krouk, G., et al. (2019). Network Walking charts transcriptional dynamics of nitrogen signaling by integrating validated and predicted genome-wide interactions. Nat. Commun. **10**:1569.

Castaings, L., Camargo, A., Pocholle, D., Gaudon, V., Texier, Y., Boutet-Mercey, S., Taconnat, L., Renou, J.P., Daniel-Vedele, F., Fernandez, E., et al. (2009). The nodule inception-like protein 7 modulates nitrate sensing and metabolism in *Arabidopsis*. Plant J. **57**:426–435.

Cheng, C.L., Dewdney, J., Nam, H.G., den Boer, B.G., and Goodman, H.M. (1988). A new locus (NIA 1) in *Arabidopsis thaliana* encoding nitrate reductase. EMBO J. **7**:3309–3314.

Chodavarapu, R.K., Feng, S., Bernatavichute, Y.V., Chen, P.Y., Stroud, H., Yu, Y., Hetzel, J.A., Kuo, F., Kim, J., Cokus, S.J., et al. (2010). Relationship between nucleosome positioning and DNA methylation. Nature **466**:388–392.

Coego, A., Brizuela, E., Castillejo, P., Ruiz, S., Koncz, C., del Pozo, J.C., Pineiro, M., Jarillo, J.A., Paz-Ares, J., Leon, J., et al. (2014). The TRANSPLANTA collection of *Arabidopsis* lines: a resource for functional analysis of transcription factors based on their conditional overexpression. Plant J. **77**:944–953.

Denyer, T., Ma, X., Klesen, S., Scacchi, E., Nieselt, K., and Timmermans, M.C.P. (2019). Spatiotemporal developmental trajectories in the *Arabidopsis* root revealed using high-throughput single-cell RNA sequencing. Dev. Cell **48**:840–852.e5.

Franco-Zorrilla, J.M., Lopez-Vidriero, I., Carrasco, J.L., Godoy, M., Vera, P., and Solano, R. (2014). DNA-binding specificities of plant transcription factors and their potential to define target genes. Proc. Natl. Acad. Sci. U S A **111**:2367–2372.

Gaudinier, A., Rodriguez-Medina, J., Zhang, L., Olson, A., Liseron-Monfils, C., Bagman, A.M., Foret, J., Abbitt, S., Tang, M., Li, B., et al. (2018). Transcriptional regulation of nitrogen-associated metabolism and growth. Nature **563**:259–264.

Gifford, M.L., Dean, A., Gutierrez, R.A., Coruzzi, G.M., and Birnbaum, K.D. (2008). Cell-specific nitrogen responses mediate developmental plasticity. Proc. Natl. Acad. Sci. U S A **105**:803–808.

Grant, C.E., Bailey, T.L., and Noble, W.S. (2011). FIMO: scanning for occurrences of a given motif. Bioinformatics **27**:1017–1018.

Guan, P., Wang, R., Nacry, P., Breton, G., Kay, S.A., Pruneda-Paz, J.L., Davani, A., and Crawford, N.M. (2014). Nitrate foraging by *Arabidopsis* roots is mediated by the transcription factor TCP20 through the systemic signaling pathway. Proc. Natl. Acad. Sci. U S A **111**:15267–15272.

Guan, P., Ripoll, J.J., Wang, R., Vuong, L., Bailey-Steinitz, L.J., Ye, D., and Crawford, N.M. (2017). Interacting TCP and NLP transcription factors control plant responses to nitrate availability. Proc. Natl. Acad. Sci. U S A **114**:2419–2424.

Gusmao, E.G., Allhoff, M., Zenke, M., and Costa, I.G. (2016). Analysis of computational footprinting methods for DNase sequencing experiments. Nat. Methods **13**:303–309.

Gutierrez, R.A., Stokes, T.L., Thum, K., Xu, X., Obertello, M., Katari, M.S., Tanurdzic, M., Dean, A., Nero, D.C., McClung, C.R., et al. (2008). Systems approach identifies an organic nitrogen-responsive gene network that is regulated by the master clock control gene CCA1. Proc. Natl. Acad. Sci. U S A **105**:4939–4944.

Hesselberth, J.R., Chen, X., Zhang, Z., Sabo, P.J., Sandstrom, R., Reynolds, A.P., Thurman, R.E., Neph, S., Kuehn, M.S., Noble, W.S., et al. (2009). Global mapping of protein-DNA interactions in vivo by digital genomic footprinting. Nat. Methods **6**:283–289.

John, S., Sabo, P.J., Thurman, R.E., Sung, M.H., Biddie, S.C., Johnson, T.A., Hager, G.L., and Stamatoyannopoulos, J.A. (2011). Chromatin accessibility pre-determines glucocorticoid receptor binding patterns. Nat. Genet. **43**:264–268.

Konishi, M., and Yanagisawa, S. (2013). *Arabidopsis* NIN-like transcription factors have a central role in nitrate signalling. Nat. Commun. **4**:1617.

Krapp, A., David, L.C., Chardin, C., Girin, T., Marmagne, A., Leprince, A.-S., Chaillou, S., Ferrario-Méry, S., Meyer, C., and Daniel-Vedele, F. (2014). Nitrate transport and signalling in *Arabidopsis*. J. Exp. Bot. **65**:789–798.

Krouk, G., Crawford, N.M., Coruzzi, G.M., and Tsay, Y.F. (2010a). Nitrate signaling: adaptation to fluctuating environments. Curr. Opin. Plant Biol. **13**:266–273.

Krouk, G., Mirowski, P., LeCun, Y., Shasha, D.E., and Coruzzi, G.M. (2010b). Predictive network modeling of the high-resolution dynamic plant transcriptome in response to nitrate. Genome Biol. **11**:R123.

Langmead, B., and Salzberg, S.L. (2012). Fast gapped-read alignment with Bowtie 2. Nat. Methods **9**:357–359.

Li, H., Handsaker, B., Wysoker, A., Fennell, T., Ruan, J., Homer, N., Marth, G., Abecasis, G., Durbin, R., and Genome Project Data Processing, S. (2009). The sequence alignment/map format and SAMtools. Bioinformatics **25**:2078–2079.

Liao, Y., Smyth, G.K., and Shi, W. (2019). The R package Rsubread is easier, faster, cheaper and better for alignment and quantification of RNA sequencing reads. Nucleic Acids Res. **47**:e47.

Liu, K.H., Niu, Y., Konishi, M., Wu, Y., Du, H., Sun Chung, H., Li, L., Boudsocq, M., McCormack, M., Maekawa, S., et al. (2017a). Discovery of nitrate-CPK-NLP signalling in central nutrient-growth networks. Nature **545**:311–316.

Liu, Y., Zhang, W., Zhang, K., You, Q., Yan, H., Jiao, Y., Jiang, J., Xu, W., and Su, Z. (2017b). Genome-wide mapping of DNase I hypersensitive sites reveals chromatin accessibility changes in *Arabidopsis* euchromatin and heterochromatin regions under extended darkness. Sci. Rep. **7**:4093.

Love, M.I., Huber, W., and Anders, S. (2014). Moderated estimation of fold change and dispersion for RNA-seq data with DESeq2. Genome Biol. **15**:550.

Maeda, Y., Konishi, M., Kiba, T., Sakuraba, Y., Sawaki, N., Kurai, T., Ueda, Y., Sakakibara, H., and Yanagisawa, S. (2018). A NIGT1-centred transcriptional cascade regulates nitrate signalling and incorporates phosphorus starvation signals in *Arabidopsis*. Nat. Commun. **9**:1376.

Marchive, C., Roudier, F., Castaings, L., Bréhaut, V., Blondet, E., Colot, V., Meyer, C., and Krapp, A. (2013). Nuclear retention of the transcription factor NLP7 orchestrates the early response to nitrate in plants. Nat. Commun. **4**:1713.

Marguerat, S., Lawler, K., Brazma, A., and Bahler, J. (2014). Contributions of transcription and mRNA decay to gene expression dynamics of fission yeast in response to oxidative stress. RNA Biol. **11**:702–714.

Medici, A., and Krouk, G. (2014). The primary nitrate response: a multifaceted signalling pathway. J. Exp. Bot. **65**:5567–5576.

Medici, A., Marshall-Colon, A., Ronzier, E., Szponarski, W., Wang, R., Gojon, A., Crawford, N.M., Ruffel, S., Coruzzi, G.M., and Krouk, G. (2015). AtNIGT1/HRS1 integrates nitrate and phosphate signals at the *Arabidopsis* root tip. Nat. Commun. **6**:6274.

Mokry, M., Hatzis, P., Schuijers, J., Lansu, N., Ruzius, F.P., Clevers, H., and Cuppen, E. (2012). Integrated genome-wide analysis of transcription factor occupancy, RNA polymerase II binding and steady-state RNA levels identify differentially regulated functional gene classes. Nucleic Acids Res. **40**:148–158.

Neph, S., Vierstra, J., Stergachis, A.B., Reynolds, A.P., Haugen, E., Vernot, B., Thurman, R.E., John, S., Sandstrom, R., Johnson, A.K., et al. (2012). An expansive human regulatory lexicon encoded in transcription factor footprints. Nature **489**:83–90.

O'Brien, J.A., Vega, A., Bouguyon, E., Krouk, G., Gojon, A., Coruzzi, G., and Gutierrez, R.A. (2016). Nitrate transport, sensing, and responses in plants. Mol. Plant **9**:837–856.

O'Malley, R.C., Huang, S.C., Song, L., Lewsey, M.G., Bartlett, A., Nery, J.R., Galli, M., Gallavotti, A., and Ecker, J.R. (2016). Cistrome and epicistrome features shape the regulatory DNA landscape. Cell **166**:1598.

Para, A., Li, Y., Marshall-Colon, A., Varala, K., Francoeur, N.J., Moran, T.M., Edwards, M.B., Hackley, C., Bargmann, B.O., Birnbaum, K.D., et al. (2014). Hit-and-run transcriptional control by bZIP1 mediates rapid nutrient signaling in *Arabidopsis*. Proc. Natl. Acad. Sci. U S A **111**:10371–10376.

Peng, H., Zhao, J., and Neff, M.M. (2015). ATAF2 integrates *Arabidopsis* brassinosteroid inactivation and seedling photomorphogenesis. Development **142**:4129–4138.

Pique-Regi, R., Degner, J.F., Pai, A.A., Gaffney, D.J., Gilad, Y., and Pritchard, J.K. (2011). Accurate inference of transcription factor binding from DNA sequence and chromatin accessibility data. Genome Res. **21**:447–455.

Pruneda-Paz, J.L., Breton, G., Nagel, D.H., Kang, S.E., Bonaldi, K., Doherty, C.J., Ravelo, S., Galli, M., Ecker, J.R., and Kay, S.A. (2014). A genome-scale resource for the functional characterization of *Arabidopsis* transcription factors. Cell Rep. **8**:622–632.

Rodgers-Melnick, E., Vera, D.L., Bass, H.W., and Buckler, E.S. (2016). Open chromatin reveals the functional maize genome. Proc. Natl. Acad. Sci. U S A **113**:E3177–E3184.

Sabo, P.J., Kuehn, M.S., Thurman, R., Johnson, B.E., Johnson, E.M., Cao, H., Yu, M., Rosenzweig, E., Goldy, J., Haydock, A., et al. (2006). Genome-scale mapping of DNase I sensitivity in vivo using tiling DNA microarrays. Nat. Methods **3**:511–518.

Sakuraba, Y., Kim, Y.S., Han, S.H., Lee, B.D., and Paek, N.C. (2015). The *Arabidopsis* transcription factor NAC016 promotes drought stress responses by repressing AREB1 transcription through a trifurcate feed-forward regulatory loop involving NAP. Plant Cell **27**:1771–1787.

Saleh, A., Alvarez-Venegas, R., and Avramova, Z. (2008). An efficient chromatin immunoprecipitation (ChIP) protocol for studying histone modifications in Arabidopsis plants. Nat. Protoc. **3**:1018–1025.

Saze, H., Kitayama, J., Takashima, K., Miura, S., Harukawa, Y., Ito, T., and Kakutani, T. (2013). Mechanism for full-length RNA processing of *Arabidopsis* genes containing intragenic heterochromatin. Nat. Commun. **4**:2301.

Sullivan, A.M., Arsovski, A.A., Lempe, J., Bubb, K.L., Weirauch, M.T., Sabo, P.J., Sandstrom, R., Thurman, R.E., Neph, S., Reynolds, A.P., et al. (2014). Mapping and dynamics of regulatory DNA and transcription factor networks in A. thaliana. Cell Rep. **8**:2015–2030.

Sung, T.Y., Chung, T.Y., Hsu, C.P., and Hsieh, M.H. (2011). The ACR11 encodes a novel type of chloroplastic ACT domain repeat protein that is coordinately expressed with GLN2 in *Arabidopsis*. BMC Plant Biol. **11**:118.

Tsay, Y.F., Ho, C.H., Chen, H.Y., and Lin, S.H. (2011). Integration of nitrogen and potassium signaling. Annu. Rev. Plant Biol. **62**:207–226.

Undurraga, S.F., Ibarra-Henriquez, C., Fredes, I., Alvarez, J.M., and Gutierrez, R.A. (2017). Nitrate signaling and early responses in *Arabidopsis* roots. J. Exp. Bot. **68**:2541–2551.

van Zanten, M., Tessadori, F., Peeters, A.J., and Fransz, P. (2012). Shedding light on large-scale chromatin reorganization in *Arabidopsis thaliana*. Mol. Plant **5**:583–590.

Varala, K., Marshall-Colon, A., Cirrone, J., Brooks, M.D., Pasquino, A.V., Leran, S., Mittal, S., Rock, T.M., Edwards, M.B., Kim, G.J., et al. (2018). Temporal transcriptional logic of dynamic regulatory networks underlying nitrogen signaling and use in plants. Proc. Natl. Acad. Sci. U S A **115**:6494–6499.

Vidal, E.A., and Gutierrez, R.A. (2008). A systems view of nitrogen nutrient and metabolite responses in *Arabidopsis*. Curr. Opin. Plant Biol. **11**:521–529.

Vidal, E.A., Araus, V., Lu, C., Parry, G., Green, P.J., Coruzzi, G.M., and Gutierrez, R.A. (2010). Nitrate-responsive miR393/AFB3 regulatory module controls root system architecture in *Arabidopsis thaliana*. Proc. Natl. Acad. Sci. U S A **107**:4477–4482.

Vidal, E.A., Moyano, T.C., Krouk, G., Katari, M.S., Tanurdzic, M., McCombie, W.R., Coruzzi, G.M., and Gutierrez, R.A. (2013a). Integrated RNA-seq and sRNA-seq analysis identifies novel nitrate-responsive genes in *Arabidopsis thaliana* roots. BMC Genomics **14**:701.

Vidal, E.A., Moyano, T.C., Riveras, E., Contreras-Lopez, O., and Gutierrez, R.A. (2013b). Systems approaches map regulatory networks downstream of the auxin receptor AFB3 in the nitrate response of *Arabidopsis thaliana* roots. Proc. Natl. Acad. Sci. U S A **110**:12840–12845.

Vidal, E.A., Alvarez, J.M., Moyano, T.C., and Gutierrez, R.A. (2015). Transcriptional networks in the nitrate response of *Arabidopsis thaliana*. Curr. Opin. Plant Biol. **27**:125–132.

Wang, R., Guegler, K., LaBrie, S.T., and Crawford, N.M. (2000). Genomic analysis of a nutrient response in *Arabidopsis* reveals diverse expression patterns and novel metabolic and potential regulatory genes induced by nitrate. Plant Cell **12**:1491–1509.

Wang, R., Tischner, R., Gutierrez, R.A., Hoffman, M., Xing, X., Chen, M., Coruzzi, G., and Crawford, N.M. (2004). Genomic analysis of the nitrate response using a nitrate reductase-null mutant of *Arabidopsis*. Plant Physiol. **136**:2512–2522.

Weirauch, M.T., Yang, A., Albu, M., Cote, A.G., Montenegro-Montero, A., Drewe, P., Najafabadi, H.S., Lambert, S.A., Mann, I., Cook, K., et al. (2014). Determination and inference of eukaryotic transcription factor sequence specificity. Cell **158**:1431–1443.

Welboren, W.J., van Driel, M.A., Janssen-Megens, E.M., van Heeringen, S.J., Sweep, F.C., Span, P.N., and Stunnenberg, H.G. (2009). ChIP-Seq of ERalpha and RNA polymerase II defines genes differentially responding to ligands. EMBO J. **28**:1418–1428.

Widiez, T., El Kafafi el, S., Girin, T., Berr, A., Ruffel, S., Krouk, G., Vayssieres, A., Shen, W.H., Coruzzi, G.M., Gojon, A., et al. (2011). High nitrogen insensitive 9 (HNI9)-mediated systemic repression of root NO3- uptake is associated with changes in histone methylation. Proc. Natl. Acad. Sci. U S A **108**:13329–13334.

Xu, N., Wang, R., Zhao, L., Zhang, C., Li, Z., Lei, Z., Liu, F., Guan, P., Chu, Z., Crawford, N.M., et al. (2016). The *Arabidopsis* NRG2 protein mediates nitrate signaling and interacts with and regulates key nitrate regulators. Plant Cell **28**:485–504.

Yang, J., Worley, E., and Udvardi, M. (2014). A NAP-AAO3 regulatory module promotes chlorophyll degradation via ABA biosynthesis in *Arabidopsis* leaves. Plant Cell **26**:4862–4874.

Yazaki, J., Galli, M., Kim, A.Y., Nito, K., Aleman, F., Chang, K.N., Carvunis, A.R., Quan, R., Nguyen, H., Song, L., et al. (2016). Mapping transcription factor interactome networks using HaloTag protein arrays. Proc. Natl. Acad. Sci. U S A **113**:E4238–E4247.

Yu, L.H., Wu, J., Tang, H., Yuan, Y., Wang, S.M., Wang, Y.P., Zhu, Q.S., Li, S.G., and Xiang, C.B. (2016). Overexpression of *Arabidopsis* NLP7 improves plant growth under both nitrogen-limiting and -sufficient conditions by enhancing nitrogen and carbon assimilation. Sci. Rep. **6**:27795.

Zhang, W., Wu, Y., Schnable, J.C., Zeng, Z., Freeling, M., Crawford, G.E., and Jiang, J. (2012a). High-resolution mapping of open chromatin in the rice genome. Genome Res. **22**:151–162.

Zhang, W., Zhang, T., Wu, Y., and Jiang, J. (2012b). Genome-wide identification of regulatory DNA elements and protein-binding footprints using signatures of open chromatin in *Arabidopsis*. Plant Cell **24**:2719–2731.

Zhong, L., Chen, D., Min, D., Li, W., Xu, Z., Zhou, Y., Li, L., Chen, M., and Ma, Y. (2015). AtTGA4, a bZIP transcription factor, confers drought resistance by enhancing nitrate transport and assimilation in *Arabidopsis thaliana*. Biochem. Biophys. Res. Commun. **457**:433–439.